Bora, CEP192 and Cenexin activate different Plk1 pools and regulate distinct cell and centrosome cycle transitions

Devashish Dwivedi[1,2*], Crisálida Borges[1,2], Daniela Harry[1,2], Luca Cirillo[3], and Patrick Meraldi[1,2*]

[1]Department of Cell Physiology and Metabolism, Faculty of Medicine, University of Geneva, 1211 Geneva 4, Switzerland

[2]Translational Research Centre in Onco-haematology, Faculty of Medicine, University of Geneva, 1211 Geneva 4, Switzerland

[3]Institute of Cancer Research, 123 Old Brompton Road, SW7 3RP, London, United Kingdom

* Correspondence to Devashish.Dwivedi@unige.ch – ORCID: 0000-0002-2039-6570 and Patrick.Meraldi@unige.ch - ORCID: 0000-0001-9742-8756

Abstract

Polo-like kinase 1 (Plk1) regulates multiple cell- and centrosome-cycle steps, including mitotic entry, DNA damage recovery, centrosome maturation and centriole disengagement. Plk1 activity depends on several independent cofactors, such as the cytoplasmic Bora, and the centrosomal Cep192 and Cenexin. However, whether these Plk1 coactivators differentially regulate the Plk1-dependent processes is unknown. Here, we show that each Plk1 co-activator controls different cell cycle steps via distinct Plk1 pools in human cells. While Bora is the main driver for mitotic entry, DNA recovery and centrosome maturation, centriole disengagement is mainly under the control of Cep192 and Cenexin. Moreover, we find that Plk1 drives S-phase progression by favouring replication origin firing, under the main control of Cep192. Our results thus uncover the complexity of Plk1 activation regulatory network, where distinct upstream activators dictate its activity in a context dependent manner.

Introduction

The Polo-like kinase 1 (Plk1) is a conserved serine/threonine kinase that controls key steps of the cell- and centrosome-cycle in animal cells to ensure faithful cell division[1]. In the mammalian cycle, Plk1 drives mitotic entry by phosphorylating and activating the Cdc25c1 phosphatase and inhibiting the Wee1 and Myt1 kinases[2-4], resulting in full Cdk1-Cyclin B activation. Plk1 activity also modulates the DNA damage response, as it essential for re-entry into the cell cycle after a DNA damage induced cell cycle arrest[5-7]. At the level of the centrosomes, Plk1 drives the dramatic increase in microtubule nucleation capacity in late G2 phase, called centrosome maturation; moreover, it is required at mitotic exit for centriole dis-engagement, the loss of the orthogonal arrangement of the two centrioles that allows centrosome duplication in the next cell cycle. Finally, in mitosis itself, Plk1 regulates multiple processes, which include nuclear envelope disassembly, chromosome condensation, spindle assembly and the stability of kinetochore microtubules[1, 8-10].

Plk1 activity and abundance shows a complex pattern in time and space. The protein consists of two halves, the N-terminal half with the kinase domain and the regulatory C-terminal half. This latter half contains a polo-box domain, which binds to Plk1 substrates via a phospho-epitope[11, 12]. During G1 and S-phase Plk1 shows little activity, as the c-terminal polo-box domain allosterically inhibits the kinase domain[13, 14]. Plk1 activity is mostly confined to the nucleus. Nevertheless, a centrosome-bound pool has been reported to promote DNA replication[15, 16]. At the onset of G2 phase, Plk1 activity rises sharply[2, 17]. During this phase it contributes to recovery from DNA damage, promotes mitotic entry and drives centrosome maturation. Plk1 activation requires the disruption of the autoinhibitory interaction between the kinase domain and the C- terminal half, which exposes its activatory T-loop for phosphorylation at Thr-210 by the mitotic kinase Aurora-A for full activation[13, 18-20]. T-loop phosphorylation by Aurora A occurs in presence of Plk1 activators, which form a tripartite complex with Aurora A and Plk1 to provide interface for phosphorylation[6, 21]. The prototypical example is Aurora borealis/Bora[22], which gets phosphorylated in the cytoplasm by Cdk1-Cyclin A, allowing it to bridge Aurora-A and Plk[19, 20, 23-25]. A similar bridging of Aurora-A and Plk1 is thought to occur at

centrosomes via the centrosomal protein Cep192[19, 20, 26, 27]. Moreover, a second centrosomal protein, Cenexin, has also been proposed to promote Plk1 activity in G2[28-30]. Thus, different Plk1 co-activators co-exist. However, the rationale behind simultaneous utilisation of multiple activators/adaptors for activating the same kinase Plk1, remains unclear. Whether they provide redundancy to Plk1 activation and serve as a fall-safe mechanism or fine-tune Plk1 activity in space and time or impart functional specialisation by regulating the activity of discreet cellular Plk1 pools, each associated with distinct cellular function, remains unclear.

Here, we show in human cells that the Plk1 activators Bora, Cep192 and Cenexin activate different pools of Plk1 and regulate distinct functions during the cell and centrosome cycle progression. While all three activators contribute to the overall Plk1 activity, cytoplasmic Bora is the key driver for DNA damage recovery, mitotic entry and centrosome maturation in late G2. In contrast, a centrosomal Plk1 activity driven by Cep192 is mainly responsible for S-phase progression. Finally, Cep192- and Cenexin-dependent Plk1 activity is required for centriole disengagement. These findings reveal that Plk1 activation is not governed by a singular mechanism but instead involves a network of upstream regulators that modulate its activity in a context-dependent manner.

Results:

Different Plk1 activators regulate the activity of distinct Plk1 pools

The Polo-like kinase plays key roles during G2. During this cell cycle phase, it localizes both to the cytoplasm/nucleoplasm and is enriched at centrosomes[31]. To test the contribution of the Plk1 activators, Bora, Cep192 and Cenexin, to the activity either of those pools we generated RPE1 cells expressing Fösters Resonance Energy Transfer (FRET) based Plk1 activity sensors[32, 33] located either in the cytoplasm/nucleoplasm or at centrosomes. In addition, these cells expressed an inducible Cyclin A2-mScarlet, allowing us, based on the presence of Cyclin A2 in the cytoplasm[17], to identify G2 cells in an asynchronous population. Applying single or combined siRNA treatments, we first found that depletion of Bora, Cep192 and Cenexin, reduced Plk1 activity in the cytoplasm/nucleoplasm and at centrosomes to the same levels seen after depletion of Aurora-A (the kinase activating Plk1[22]) or treatment with a Plk1 inhibitor BI2536[34]. This confirmed that these three proteins are the main Plk1 activators (Fig. 1A-D). Second, we found that Plk1 activity in the cytoplasm/nucleoplasm was primarily, but not exclusively, dependent on Bora, whereas the centrosomal Plk1 pool was primarily dependent on the centrosomal activators Cep192 and Cenexin (Fig. 1A-D and S1A-D; Validation of depletion S1E-G). These results suggest that Plk1 activation by Bora, Cep192 and Cenexin occurs in a compartmentalized manner, where Bora regulates the activity of cytoplasmic/nucleoplasmic Plk1 pool and Cep192 and Cenexin regulate Plk1 activity on the centrosomes. Nevertheless, the fact that Plk1 activity at either pool could only be suppressed after depletion of all three co-activators, suggested a continuous exchange of Plk1 between these two localisations.

Plk1 localisation is dynamic on the centrosome

To test for the exchange between the cytoplasmic/nucleoplasmic pool and the centrosomal pool, we recorded the dynamics of Plk1 recovery on centrosomes after photobleaching (FRAP) in RPE1 cells expressing endogenously tagged GFP-Plk1. FRAP-recordings of control-depleted cells in which

centrosomal GFP-Plk1 was bleached, indicated the presence of at least two GFP-Plk1 pools: 2/3 of GFP-Plk1 rapidly exchanged with the cytoplasmic pool with a $t_{1/2}$ value of less than 10s, while 1/3 of GFP-Plk1 was immobile over a period of 3 minutes (Fig. 2A-B and Supplementary Video 1). To test to which extent this immobile pool depended on Cep192 and Cenexin, we depleted either protein or in combination. We found that the immobile fraction diminished in the depletion in either of the two centrosomal co-activator, and that it was abolished in the Cep192/Cenexin co-depletion (Fig. 2C-I and Supplementary Videos 2-4). This change in the mobility was due to a change in Plk1 activators, since Plk1 inhibition had no effect on the relative fraction of mobile and immobile Plk1 (Fig. 2J and S2A-D and Supplementary Video 5-6). Finally, we also tested whether Bora, Cep192 or Cenexin-depletion affected the overall abundance of GFP-Plk1 at centrosomes and found that all three depletions led to a moderate reduction in Plk1 levels (Fig. 2K-L and S2E-F), consistent with the previous observation that Plk1 activity can regulate the overall abundance at centrosomes. We conclude that in G2 the majority of the centrosomal pool of Plk1 can exchange with the cytoplasm/nucleoplasm, and that a smaller part of the centrosomal pool is immobile, most likely bound to Cep192 and Cenexin.

Plk1 activity on the centrosomes is essential for timely progression of S-phase

Plk1 activity is crucial for progression through different cell cycle stages[1]. We therefore investigated how the depletion of Bora, Cep192 and Cenexin affect the duration of S and G2 phases. We performed long-term time lapse imaging of live RPE1 cells expressing endogenously tagged mRuby-PCNA which enabled us to distinguish between the different cell cycle phases. Control-depleted cells completed their S phase in 3.88±1.21 h and G2 in 4.59±1.32 h (Fig. 3A-B and 4A-B; Supplementary Video 7 and 8). Depletion of Cyclin A2, a critical regulator of S- and G-phase and our positive control, strongly delayed, as expected, S-phase and nearly completely blocked the G2/M transition, as 95% of the cells failed to enter mitosis (Fig. 3A-B, and 4A-B; Supplementary Video 9 and 10). The depletion of any of the three Plk1 co-activator significantly increased S-phase duration, with Cep192 depletion resulting in the strongest delay (9.57±2.85 h; Fig. 3A-B; Supplementary Video 11-13); in

contrast only Bora depletion led to a significant delay during G2 (13.99±6.48 h; Fig. 4A-B, Supplementary Video 19-21). Co-depletion of the other co-activators did not further delay S-phase when compared to Cep192 depletion, or further delay G2 completion when compared to Bora depletion (Fig. S3 A-D; Supplementary Video 14-26). Visual inspection of the mRuby-PCNA signal, which reflects replication origin firing in S-phase[39], suggested a reduction in this activity; moreover, previous indicated that *Xenopus laevis* Plk1 regulates DNA replication origin firing in embryonic extracts[35-37]. To test if this is also the case in human somatic cells, we depleted Bora, Cep192 or Cenexin, synchronised the cells at G1/S boundary with the Cdk4/6 inhibitor Palbociclib (Cdk4/6i)[38], released them for 3 hrs to reach mid S phase, stained them for PCNA, and counted the number of foci per nucleus. While Cep192 depletion resulted in around four-fold reduction in the number of PCNA foci, Bora depletion had a mild effect and Cenexin depletion did not result in any change (Fig 3C-D). Overall, we conclude that the cytosolic Plk1 activator Bora is rate-limiting for the timely progression of G2 phase, whereas the centrosomal Plk1 activator Cep192 is critical for replication origin firing and timely completion of S-phase.

Cep192 regulates both cellular and centrosomal Plk1 activity during S phase

Cep192 acts as a scaffold for Aurora A dependent Plk1 activation[19, 20, 26, 27], but has been also been shown to affect centrosome duplication during S-phase[40, 41]. To distinguish if the prolonged S phase observed after Cep192 depletion is due to centriole duplication defects or due to loss of Plk1 activity, we generated cells without centrosomes. Specifically, we blocked centrosome duplication with the Plk4 inhibitor centrinone[42] in RPE1 cells lacking USP28, a component of the mitotic stopwatch checkpoint which induces a p53-dependent cell cycle arrest after centrosome loss[43]. After a 1-week centrinone treatment and a single cell selection, we obtained a RPE1 *USP28*$^{-/-}$ cell line devoid of any centrosomes (Fig. S4A-B). Flow cytometry indicated that same proportion of RPE1, RPE1 *USP28*$^{-/-}$ and RPE1 *USP28*$^{-/-}$ devoid of centrosomes in G1-, S- or G2/M-phase; (Fig. 5A-C); nevertheless, Cep192 depletion in RPE1 *USP28*$^{-/-}$ devoid of centrosomes still led to an S-phase enrichment (Fig.

5D), suggesting that Cep192 drives the S-phase progression via Plk1 activity and independently of centrosomes.

We therefore we also quantified the cellular and the centrosomal activity of Plk1 during S phase after Bora, Cep192 or Cenexin depletion. Using the nuclear localisation of Cyclin A2 as proxy[17] to identify S phase cells we first found that the cytoplasmic Plk1 activity was much higher in G2 compared to S-phase, but that the centrosomal Plk1 activity was equivalent in both phases (Figure 5E-H). Moreover the Plk1 activity in S-phase at either site depended on Cep192, but not on Bora or Cenexin (Figure 5E-H). This suggested that Cep192 is the main initiator of both cytoplasmic and centrosomal Plk1 activity in S-phase (Figure 5E-H).

Bora is essential for DNA-damage recovery

In addition to its generic cell cycle roles, Plk1 is also critical for cell cycle re-entry after DNA damage, as it directly inhibits the DNA damage checkpoint effectors 53BP1, p53 and their downstream checkpoint kinases Chk1 and Chk2[44-47]. To determine which Plk1 activator regulates checkpoint recovery after DNA damage, we depleted Bora, Cep192 and Cenexin, synchronised the cells at the G1/S boundary with a Cdk4/6i, released them for 6 hours in the presence or absence of a short pulse of the DNA-damaging agent Doxorubicin , and treated them with the Eg5 inhibitor STLC for 16 hours, to arrest them in mitosis (See scheme Fig. 6A). By determining the mitotic index, we could monitor the ability of cells to recover from a DNA-damage induced cell cycle arrest. Consistent with previous studies, Bora depletion specifically abolished mitotic entry after a Doxorubicin pulse, indicating a failure to recover from a DNA damage-induced cell cycle arrest (Fig. 6B-C; Confirmation of DNA damage in Fig. S6A). In contrast, Cenexin depletion did not prevent mitotic entry (Fig. 6B-C). Cep192 depletion and complete Plk1 inhibition gave inconclusive results, as those two perturbations already prevented mitotic entry in the absence of Doxorubicin pulse (Fig. 6D-E and S6B-C), most likely reflecting their key contribution to S-phase progression. We conclude that Bora-dependent Plk1 activity, but not Cenexin, are required for DNA-damage recovery.

Bora is the major driver of Plk1 dependent centrosome maturation during late G2

As cells prepare for mitotic entry in late G2, Plk1 drives centrosome maturation via the recruitment of pericentrosomal matrix (PCM) proteins such as Pericentrin (PCNT) and γ-tubulin, to increase their the microtubule nucleation capacity of the future spindle poles[48-51]. To identify the contribution of each of the Plk1-adaptors in this process, we monitored the total volume of γ-tubulin and PCNT on the early prometaphase spindle poles after Bora, Cep192 or Cenexin depletion. Whereas Bora-depletion reduced the levels of γ-tubulin and PCNT on spindle poles as severely as Plk1 depletion, Cep192 depletion only led to an intermediate (50%) reduction, and Cenexin depletion had no effect (Fig. 7A-C and S7A-C). This indicated that the cytoplasmic pool of Plk1, under the control of Bora, is the key regulator of centrosome maturation.

Centriole disengagement is driven by Cep192 and Cenexin

In cells exiting mitosis, Plk1 regulates the first step of centrosome duplication by inducing centriole disengagement during mitotic exit[52-54]. In our previous work, we had shown that an incomplete activation of Plk1, due to mild DNA replication stress, led to premature centriole disengagement in G2[55]. We hypothesized that such a partial Plk1 activity mimics the condition found during mitotic exit, when Plk1 activity declines[56]. To analyse how this process is controlled, we depleted each of three Plk1 activator, and analysed the engagement status of centrioles in G2 phase using Ultrastructure-Expansion Microscopy (U-ExM), as described previously[55].

Strikingly, Bora depletion led to premature centriole disengagement in nearly all cells (98.10±1.65% vs. 1.76±1.61% in control-depleted cells), while Cep192 depletion had an intermediate effect (3.10±3.95% of cells with disengaged centrioles), while Cenexin loss did not induce centriole disengagement (Fig. 8A-C). Premature centriole disengagement was not due to DNA replication stress, since in contrast to the DNA-polymerase inhibitor aphidicolin, none of the depletions led to an increase in typical markers of DNA replication stress, such as 53BP1 or γ-H2AX foci (Fig. S8A-C). These results suggested that in conditions of partial cytoplasmic Plk1 activity but high

centrosomal Plk1 activity, as seen after Bora depletion, centrioles will disengage (Fig 1). To test this hypothesis we co-depleted Bora and CEP192 either in WT RPE1 cells or in RPE1 *CENEXIN*$^{-/-}$ knock-out cells (to avoid applying a technically difficult triple siRNA treatment), and found that loss of either of the two centrosomal Plk1 activators indeed reduced centriole dis-engagement in a Bora siRNA background, and that the depletion of both centrosomal activators nearly completely abolished premature centriole dis-engagement (Fig. 8A-C). We conclude that centriole disengagement is driven mostly by the centrosomal Plk1 activators Cep192 and Cenexin, and a condition with partial cytoplasmic Plk1 activity but high centrosomal Plk1 activity in G2 is sufficient to induce premature centriole dis-engagement.

Finally, we quantified the proteolytic Separase activity in the depletion leading to premature centriole disengagement. Indeed, in addition to Plk1 , Separase plays a key role in inducing centriole disengagement both during telophase[57-59] and during G2 in response to mild replication stress[55]. We used an established Separase activity sensor[60] to monitor the Separase activity on centrosomes during G2 phase, and found that unlike mild replication stress induced by low doses of Aphidicolin (positive control), none of the conditions revealed an upregulated Separase activity on centrosomes (Fig. 8D-E). This suggested that centriole disengagement observed after the depletion of Bora and Cep192 purely rely on partial Plk1 activity.

Discussion

Here we investigated how the different Plk1 co-activators regulate Plk1 activity in time and space and whether they differentially control the Plk1-dependent transitions of the cell- and centrosome-cycle. In terms of spatial regulation, our results indicate that the centrosomal and the cytoplasmic Plk1 pools are under the control of distinct Plk1 co-activators, but that a partial exchange exists between the two populations. At the functional level, we demonstrate that the Plk1-dependent cell- and centrosome cycle steps are differentially regulated by each Plk1 coactivator. Cytoplasmic Bora is the main driver for mitotic entry, DNA recovery and centrosome maturation, while centriole disengagement is controlled by the centrosomal co-activators Cep192 and Cenexin. Moreover, we uncover that replication origin firing and S-phase progression specifically depends on the centrosomal activator Cep192, which initiates Plk1 activation both at centrosomes and the cytoplasm.

Our results indicate that the cytoplasmic and centrosomal pools of Plk1 activity are under distinct control. While in G2 Bora is the main activator of the cytoplasmic Plk1 pool, Cep192 and Cenexin are largely responsible for the activity of the centrosomal Plk1 pool. This indicates that both Plk1 pools must be considered separately. This is in agreement with previous studies which indicated that DNA-damage recovery is under the control of cytoplasmic Plk1, but not nuclear Plk1 or a Plk1 version that cannot diffuse from centrosomes[15] or that kinetochore-microtubule attachments are regulated specifically by a kinetochore-bound form of Plk1[61]. Nevertheless, our FRET and FRAP measurements also indicate a partial diffusion of Plk1 protein and activity between the cytoplasmic and centrosomal pools, consistent with previous studies[62, 63]. Indeed, our data revealed an exchangeable pool and a static Plk1 tool at centrosomes, that depends on Cep192 and Cenexin, in contrast to a previous study, which reported only an exchangeable pool[63]. This difference may the consequence of different Plk1 expression levels as we studied the endogenous protein, compared to an exogenously tagged version in previous studies.

A second major conclusion of this study is that the each Plk1 activator differentially regulates the Plk1-dependent cell- and centrosome cycle transitions. While Bora is the main driver of mitotic entry,

DNA damage recovery, and centrosome maturation, we uncover a major role of Cep192 in S-Phase progression and centriole disengagement, and a restricted role for Cenexin in centriole disengagement. Earlier studies reported negligible Plk1 activity during early cell cycle phases and proposed that Plk1 activation is restricted to late G2 phase, requiring S-phase completion[2, 17, 21]. Other studies, nevertheless, pointed to emerging evidence of a role of Plk1 in DNA replication[5, 35-37]. Our data indicate that human cells have a low, but important Plk1 activity in S-Phase that drives DNA replication origin firing. This S-phase activity depends on Cep192, an activator that is thought to recruit Aurora A and Plk1 to centrosomes to drive centrosome maturation and spindle formation[26, 64], but not on centrosomes themselves. The most logic conclusion is that Plk1 activity in S-phase depends mainly on Cep192 activation, but that this interaction is not dependent on this particular localization. Whether this S-phase activation depends on Aurora-A, remains to be seen.

As the cells progress to G2, Bora becomes the main Plk1 activator, consistent with the parallel activation of Aurora A[67]. Our data is consistent with previous findings on the critical role of Plk1 in regulating DNA damage checkpoint recovery, centrosome maturation and mitotic entry at late G2[22, 25, 50]. Our data show a similar magnitude of impaired centrosome maturation after depletion of either Bora or Plk1. This implies that Cep192 and Cenexin cannot substitute for cytoplasmic Bora during centrosome maturation, despite being bound to centrosomes. We still did observe a partial impairment of centrosome maturation in Cep192 depleted cells, consistent with a direct role of Cep192 in centrosome cycle progression[69-72], but this activity is not sufficient to drive centrosome maturation on its own. This suggest that for full centrosome maturation, Plk1 may also need to phosphorylate other critical regulators of centrosome maturation in the cytoplasm.

Finally, Plk1 is responsible for centriole disengagement[52, 54], a critical step for licensing the centrioles for next round of duplication. We noted that this appears to be the only step that depends on the Cep192 and Cenexin dependent centrosomal pool of Plk1. Our data indicates that Cep192 is the primary activator for centrosomal Plk1 pool and Cenexin only has limited contribution towards fine-tuning centrosomal Plk1 activity. This aligns with a recent study revealing the role of Cenexin in fine-

tuning centrosome maturation on old and new centrosomes through Plk1 activity[30]. Centriole disengagement which normally occurs during telophase appears to be predominantly regulated be Cep192 and Cenexin dependent centrosomal Plk1 pool as Bora is degraded in mitosis[21, 73, 74]. This is also consistent with our previous finding that the Plk1 activity threshold required for centriole disengagement is much lower[55] compared to other mitotic steps that require full Plk1 activation.

Overall, we demonstrate that relying on different Plk1 activators for different Plk1-dependent steps creates a sophisticated regulatory network coordinating distinct steps during mitotic progression. This differential system has, however, also the potential to induce genetic instability, as observed in case of Bora depletion where the mitotic progression is delayed while the centrosome cycle is advanced, leading to a severe desynchrony between the two otherwise synchronous cell and centrosome cycle. It therefore will be interesting to examine in the future, whether such type of asychronicities can also be observed in pathological conditions, such as the genetically instable cancer cells.

Methods

Cell culture and drug treatments: hTERT-RPE1 cells (ATCC: CRL-4000), hTERT-RPE1 Plk1-GFP, hTERT-RPE1 USP28 KO (kind gift by Arshad Desai, University of California, San Deigo, United States)[43], h-TERT RPE1 Cenexin KO (kind gift by gift of Brian Tsou, Memorial Sloan Kettering Cancer Centre, Sloan Kettering Institute, United States)[75], hTERT-RPE1 mRuby-PCNA (kind gift by Alexis Barr, Imperial College London, United Kingdom)[76], hTERT-RPE1 Plk1-EGFP (kind gift by Monica Gotta, University of Geneva, Switzerland), hTERT-RPE1 Cyclin A2-mScarlet + Plk1-FRET Sensor, hTERT-RPE1 Cyclin A2-mScarlet + Plk1-FRET-PACT sensor, hTERT-RPE1 Separase Sensor cells were cultured in Dulbecco's Modified Eagle's Medium (Thermo Fisher Scientific: 61965-026) supplemented with 10% foetal calf serum (FCS) [Regular: (Thermo Fisher Scientific: A5256701) or Tet-System Approved: (Thermo Fisher Scientific: A4736201) as required] and 100U/ml of each penicillin and streptomycin (P/S) (Thermo Fisher Scientific: 15140122) at 37°C, 95% relative humidity and 5% CO_2 in humidified CO_2 incubator. All cell lines were routinely tested for mycoplasma contamination by PCR. For live-cell imaging, cells were cultured in Leibovitz's L-15 medium without Phenol Red (Thermo Fischer Scientific: 21083-027) with 10% FCS and 100 U/ml P/S at 37°C. Cells were treated with following inhibitors/drugs to inhibit/induce indicated proteins as per experimental requirement, Cdk1: 9 µM RO3306 (Sigma Aldrich: SML0569), Plk1: 10 nM BI2536 (Selleck Chemicals: S1109), 300 nM Plk4: Centrinone (Tocris Bioscience: 5687), Eg5: 10 µM (+)-S-Trityl-L-cysteine/STLC (Sigma Aldrich: 164739), DNA polymerase (to induce mild replication stress): 400 nM Aphidicolin (Sigma Aldrich: A0781) and 1 µg/ml Doxycycline (Sigma Aldrich: D3447-1G). To label microtubules and DNA in live cell imaging 50 nM SiR-Tubulin (Cytoskeleton Inc: CY-SC002), SiR-DNA (Cytoskeleton Inc: CY-SC007) and SPY505-DNA (Cytoskeleton Inc: CY-SC101) were used according to manufacturer's instructions.

Preparation of stable cell lines: hTERT-RPE1 Separase sensor cells were prepared by transfecting hTERT-RPE1 FRT/TR cells with 0.5 µg Separase Sensor (pcDNA5-FRT/TO- mCherry-Scc1$^{(142-467)-\Delta NLS}$-eGFP-PACT)[60] and 4.5 µg pOG44 plasmids using X-tremeGENE™ 9 (Merck: XTG9-RO) transfection reagent according to manufacturer's instructions. The transfected recombinants were selected with 200 µg/ml Hygromycin-B (Invivogen: ant-hm-5) in DMEM with 10% FCS and 100 U/ml P/S. A two-tiered approach was used to prepare hTERT-RPE1 Cyclin A2-mScarlet + Plk1-FRET Sensor and hTERT-RPE1 Cyclin A2-mScarlett + Plk1-FRET-PACT (Centrosome localised) sensor cells, where first hTERT-RPE1 FRT/TR cells were transfected with 0.5 µg Cyclin A2 (pcDNA5-FRT/TO-Cyclin A2-mScarlet) and 4.5 µg pOG44 plasmids as described above to generate hTERT-RPE1 Cyclin A2-mScarlet cells. These cells were later transfected again with either Plk1-FRET sensor c-jun substrate plasmid [32] (Addgene Plasmid # 45203) or c-jun based Plk1 FRET sensor tagged to PACT domain at c-terminus enabling centrosomal localisation [33] (Addgene Plasmid #

Plasmid #106907) using X-tremeGENE™ 9 (Merck: XTG9-RO) transfection reagent according to manufacturer's instructions. Transfected cells were selected with DMEM with 10% FCS (Tet-System compatible) and 100U/ml P/S supplemented with both 600 µg/ml of G418 (Invivogen: ant-gn-5) and 200 µg/ml Hygromycin-B (Invivogen: ant-hm-5) followed by single cell cloning. Centrosome less USP28 KO cells were prepared by prolonged Plk4 inhibition followed by clonal selection of cells devoid of centrioles. These cells were constantly maintained with Plk4 inhibitor to prevent de-novo centriole formation.

RNA Interference: siRNA transfections were performed using Lipofectamine RNAiMAX (Thermo Fisher Scientific: 13778075) according to manufacturer's instructions. RNAi was performed for 72 h; when combined with inhibitors the drugs were added 60 hours post transfection. All the siRNA sequences used in the study were previously validated sequences: siControl (Qiagen, GGACCTGGAGGTCTGCTGT), siBora (Dharmacon, TAACTAGTCCTTCGCCTATTT) [73], siCep192 (Dharmacon, AAGGAAGACATTTTCATCTCTTT), siCenexin (Dharmacon, GGCACAACATCGAGCGCAT), siCyclin A2 SMARTpool (Dharmacon, GGAAATGGAGGTTAAATGT, TAGCAGAGTTTGTGTACAT, ATGAGGATATTCACACATA, TGATAGATGCTGACCCATA), siAurora-A (Dharmacon, ATGCCCTGTCTTACTGTCA), siPlk1 (Dharmacon, CGAGCTGCTTAATGACGAG), siSeparase (Dharmacon, GCTTGTGATGCCATCCTGA) [77].

Antibodies: The following antibodies were used in this study: Mouse anti-α-tubulin (Geneva antibody facility: AA345-M2a; 1:250: ExM) [78], Mouse anti-β-tubulin (Geneva antibody facility: AA344-M2a; 1:250: ExM) [78], Mouse anti-α-tubulin (Clone: DM1α, Sigma Aldrich, T9026, 1:5000: Western Blotting), Bora (gift from Erich Nigg, 1:1000 Western blotting)), CEP192 (Bethyl: A302-324A, 1:1000 Western blotting), Cenexin (abcam: ab43840, 1:1000 Western blotting) , Aurora A (BD Biosciences: 610939, 1:1000 Western blotting), Plk1 (abcam: ab17057, 1:1000 Western blotting), Rabbit polyclonal anti-Pericentrin (abcam: ab4448; 1:250: ExM, 1:2000: IF), Mouse anti-Cyclin A2 (Clone: E32.1, abcam: ab38; 1:1000: Western Blotting), Chicken anti-GFP (Thermo Fisher Scientific: A10262; 1:2000 IF) and Mouse monoclonal anti-Separase (abcam: ab16170; 1:500 Western blotting). All the Alexa Fluor-conjugated secondary antibodies were purchased from Thermo Fisher Scientific and used at 1:500 dilution. For Immunoblotting experiments, Horeseradish Peroxidase (HRP)-Conjugated goat anti-mouse antibody was purchased from Thermo-Fisher (Cat # 32430) and HRP-Conjugated goat anti-rabbit antibody was purchased from BioRad (Cat# 1706515) and both of them were used at 1:10,000 dilution.

FRET assay to measure Plk1 activity: Tetracycline inducible hTERT-RPE1 Cyclin A2-mScarlett Cells stably and constitutively expressing Plk1 FRET sensor were seeded in four-well glass bottom µ-Slide Ibidi chambers (Ibidi; 80426) and treated with different inhibitors/siRNAs as indicated in

DMEM with 10% FCS and 1% P/S. The DMEM was replaced with Leibovitz L-15 supplemented with 10% FCS and 1% P/S containing same inhibitors as before if any. The chambers were acclimatised in 37 °C chamber before imaging. The acquisition was performed with an EC Plan Apochromat 100X (NA 1.56) oil objective on a Zeiss Cell Observer.Z1 spinning disk microscope (Nipkow Disk) equipped with a 37 °C chamber and a CSU X1 automatic Yokogawa spinning disk head. To perform FRET experiments samples were illuminated with 445 nm laser and the emission signal was split equally using DV2 split view system and CFP and YFP emissions were recorded on the split beams. 512×512-pixel size images were acquired with an Evolve EM512 camera (Photometrics) using Visiview 4.00.10 software. Acquired images were analysed using ImageJ to calculate the YFP to CFP emission intensity ratio after background subtraction.

Immunofluorescence: Cells treated with indicated inhibitors/siRNAs were fixed in prechilled methanol at -20°C for 6 min. Fixed cells were blocked in Blocking solution (5% BSA in PBS), followed by incubating with indicated primary and secondary antibodies for 1 h and 30 min, respectively, with three washes of 10 min with PBS in between. Stained coverslips were mounted on glass slides with Vectashield with DAPI (Vector Laboratories: H-1200-10) and visualised using 100x PLAN Apochromat oil-immersion (NA 1.4) objective on an Olympus DeltaVision microscope (GE Healthcare) equipped with a DAPI/FITC/Rhodamine/CY5 filter set (Chroma Technology Corp) and a CoolSNAP HQ camera (Roper-Scientific). The three- dimensional image stacks were deconvolved with SoftWorx (GE Healthcare). The acquired images were cropped and processed with ImageJ (NIH) software to generate intensity projections (maximum/average) and extract fluorescence intensity and pixel size values according to the analysis requirement.

Immunoblotting: Cells were grown in 60 mm plastic dishes and treated with inhibitors/drugs overnight. To prepare protein lysate the cells were scrapped off using cell scrapper and lysed in RIPA buffer (50 mM Tris pH-7.4, 150 mM NaCl 1% Nonidet P-40 (Thermo Fisher Scientific: 85124), 0.5% Sodium deoxycholate (Sigma Aldrich: D5670), 0.1% Sodium dodecyl-sulphate in ultrapure water) supplemented with Protease inhibitor (Roche: 11873580001) and Phospho-STOP (Roche: 04906845001). Protein concentrations in the lysates were determined using the Bradford Protein Assay (Thermo Fisher; 23200). Samples with equal amounts of protein were mixed with 4X Laemmli buffer and heated to 95 °C for 5 min. Proteins were separated on a 10% SDS-polyacrylamide gels and transferred onto a 0.45 µm pore size nitrocellulose membrane (Macherey-Nagel GMBH: 741280) by wet blotting. Membranes were blocked with 5% non-fat dry milk in TBS 0.1% Tween20 (TBS-T) for 30 min. After blocking, membranes were incubated with primary antibodies overnight at 4 °C in TBS-T 5% non-fat dry milk. Membranes were washed three times with TBS-T and incubated 1 h with the appropriate peroxidase-conjugated secondary antibody in TBS-T 5% non-fat dry milk. The membranes were washed thrice with TBS-T and the bands corresponding to protein of interest were

detected by chemiluminescence using the Amersham ECL Prime Western Blotting Detection Kit (GE Healthcare; RPN2232) in a Fusion FX7 Spectra Multispectral Imaging system (Witec AG, Switzerland).

Live cell imaging and analysis: For live cell imaging experiments hTERT-RPE1 cells endogenously tagged with mRuby-PCNA were plated in glass bottom Ibidi chambers (Ibidi GMBH: Cat # 81158) and normal DMEM medium was replaced with L15 Leibovitz's medium supplemented with 10% FCS, 100 U/ml P/S, 50 nM SiR-Tubulin and 100 nM SPY505-DNA prior to imaging. The cells were treated with indicated inhibitors/siRNAs and imaged at 37 °C on a Nikon Ti microscope equipped with a 60x NA 1.3 oil objective, DAPI/FITC/Rhodamine/CY5 (Chroma, USA) filter set, Orca Flash 4.0 CMOS camera (Hamamatsu, Japan) and the NIS software. Cells were recorded every 10 min for 48 h with z-slices separated by 1 µm, and 100 ms exposure per z-slice at wavelengths of 488 (525), 561 nm (615 nm) and 647 (670) excitations (emission). The time-lapse movies were analysed manually for the duration of S and G2 phases based on PCNA localisation using Imaris software (Bitplane Inc).

Flow cytometry-based cell cycle profile analysis: Asynchronously growing cells in log phase were collected by trypsinisation in a microcentrifuge tube, counted and fixed with prechilled 70% ethanol and incubated overnight at -20°C. Next day, the cells were washed with 1X PBS and resuspended in PI/RNase Staining Buffer (BD Biosciences: 550825) to a final concentration of 0.5 million cells per ml of suspension and incubated in dark for 1h at room temperature. The DNA content in the cells was analysed on CYTOFLEX flow cytometer (Beckman Coulter) using 561 nm laser after removing the doublets. The acquired data was analysed in FlowJo 10 Software (BD Biosciences) to extract the percentage of cells in different cell cycle stages based on DNA content.

Expansion microscopy: Cells were grown on 12 mm circular glass coverslips (Thermo Fisher Scientific) and treated with required inhibitors/drugs overnight. Next day the coverslips were treated with Acrylamide (AA)-Formaldehyde (FA) Solution [1.4% AA (Sigma Aldrich: A4058) and 2% FA (Sigma Aldrich: F8775) in PBS] for 5 h at 37°C to prevent protein crosslinking. Coverslips were next subjected to gelation by incubation for 1 hr at 37°C with monomer solution [19% Sodium Acrylate (Sigma Aldrich: 408220), 10% Acrylamide, 0.1% Bisacrylamide (Sigma Aldrich: M1533), 0.5% Tetramethyl ethylenediamine-TEMED (Thermo Fisher: 17919), 0.5% Ammonium Persulfate (Thermo Fisher: 17874) in PBS]. Post gelation, the coverslips were treated with denaturation solution [50 mM Tris (Sigma Aldrich: 99362), 200 mM Sodium dodecyl sulphate (Axon Lab AG: A2572.0500), 200 mM Sodium Chloride (Axon Lab AG: A3597.1000) in Nuclease free water, pH: 9.0] for 15 min on a rocker shaker at room temperature to detach the gels from coverslips. The gels were heated at 95°C for 90 min in denaturation solution followed by three 30 min washes with water. The gels were incubated with PBS for 15 min followed by 3 hrs incubations with primary and

secondary antibodies followed each by three 10 min washes at 37°C and gentle shaking. Stained gels were kept overnight in water for optimal expansion. The size of gel was measured to calculate the expansion factor and the gel was cut into small pieces and placed in 2 well plastic bottom ibidi chamber (Ibidi GMBH: Cat # 80286)- The 3D image stacks of centrioles in G2 phase cells (4 centrioles in one cell) were acquired in 0.1 µm steps using a 100x PLAN-Apochromat oil-immersion (NA 1.4) objective on an Olympus DeltaVision microscope (GE Healthcare) equipped with a DAPI/FITC/Rhodamine/CY5 filter set (Chroma Technology Corp) and a CoolSNAP HQ camera (Roper-Scientific). The three- dimensional image stacks were deconvolved with SoftWorx (GE Healthcare). The acquired images were cropped and processed with ImageJ (NIH) software to construct 3D image to analyse the configuration of centrioles (orthogonal orientation and distance in between) for each image.

Separase Activity Measurements: Separase activity measurements were performed on live cells. hTERT-RPE1 cells expressing Separase sensor were plated in glass bottom Ibidi chambers (Ibidi GMBH: Cat # 81158) and DMEM containing Tet-System approved FCS and transfected with indicated siRNAs. DMEM was replaced with L15 Leibovitz's medium supplemented with 10% FCS, 100 U/ml P/S, 50 nM SiR-DNA and 1 µg/ml Doxycycline 3 hrs prior to imaging. Cells with two distinct centrosomes and intact nucleus (G2 phase) were selected and 3D image stacks of centrosomes were acquired for FITC, TRITC and Cy5 channels in 0.1 µm incremental z-steps using a 100x oil-immersion (NA 1.4) objective on an Olympus DeltaVision microscope (GE Healthcare) equipped with a DAPI/FITC/Rhodamine/CY5 filter set (Chroma Technology Corp) and a CoolSNAP HQ camera (Roper-Scientific). The three- dimensional image stacks were deconvolved with SoftWorx (GE Healthcare). The acquired images were cropped and processed with ImageJ (NIH) software to extract the intensities of GFP and mCherry in the centrosomes for each image and plotted as the ratio of GFP to mCherry as the measure of Separase activity.

Statistical analysis: Statistical tests for all figures were performed using GraphPad Prism 10 (GraphPad), the statistical tests employed in every case are described in the figure legends. Minimum three independent biological replicates were performed in all experiments.

Acknowledgements

Authors thank M. Gotta (University of Geneva, Switzerland) for cell lines, E. Schiebel (University of Heidelberg) for plasmid constructs, P. Guichard, M. Laporte and V. Hamel (University of Geneva, Switzerland) for expansion microscopy support, Members of Bioimaging and FACS facility (University of Geneva, Switzerland) for experimental support, Monica Gotta and team (University of Geneva, Switzerland) and members of Meraldi laboratory for helpful discussions and support.

Competing interests

The authors declare no competing or financial interests.

Author contributions

Conceptualization: D.D., P.M.; Formal analysis: D.D., C.B., L.C. P.M.; Investigation: D.D., C.B. L.C. D.H.; Writing - original draft: D.D.; Writing - review & editing: D.D., P.M.; Visualization: D.D.; Supervision: P.M.; Project administration: P.M.; Funding acquisition: D.D., P.M.

Funding

This work was supported by the Swiss National Science Foundation (Schweizerischer Nationalfonds zur Förderung der Wissenschaftlichen Forschung; SNF) project grant (No. 31003A_208052) to P.M., Novartis Foundation for Biomedical Research, Young Investigator Grant (No. 23A015) to D.D., Foundation NOVA Project Grant to D.D., and the Université de Genève.

Figure Legends:

Figure 1: (A) Representative images of G2 phase hTERT-RPE1 cells expressing cellular Plk1 activity sensor and Cyclin A2-mScarlet treated with indicated siRNAs or inhibitors. **(B)** Box and Whisker plot for FRET measurement-based quantification of cellular Plk1 activity calculated from G2 phase cells represented in **(A)** derived from N=3 independent experiments comprising n= 115: siControl, 124: siBora, 117: siCep192, 122: siCenexin, 132: siCep192 + siCenexin and 125: Plk1i cells. **(C)** Representative images of G2 phase hTERT-RPE1 cells expressing centrosomal Plk1 activity sensor and Cyclin A2-mScarlet treated with indicated siRNAs or inhibitors. **(D)** Box and Whisker plot for FRET measurement-based quantification of centrosomal Plk1 activity calculated from G2 phase cells represented in **(C)** derived from N=4 independent experiments comprising n= 183: siControl, 183: siBora, 181: siCep192, 183: siCenexin, 185: siCep192 + siCenexin and 192: Plk1i cells. Data presented as the entire range with values between first and third quartiles in boxes. '+' sign in each column represent the mean value (p values for individual comparisons indicated on graphs: Kruskal-Wallis test). Scale bars = 5 µm.

Figure 2: (A-H) Representative time stamp images and quantifications from FRAP movies from G2 phase Plk1-EGFP tagged hTERT-RPE1 cells treated with non-targeting siRNA control **(A;** quantification of recovery in **(B))**, Cep192 siRNA **(C** quantification of recovery in **(D))**, Cenexin siRNA **(E** quantification of recovery in **(F))** and siCep192 + siCenexin **(G** quantification of recovery in **(H))**. **(I)** Box and Whisker plot for measurement of mobile Plk1 pool on centrosomes under indicated conditions (N=3 independent experiments; n= 43, 44, 43 and 45 for siControl, siCep192, siCenexin and siCep192 + siCenexin, respectively.) **(J)** Box and Whisker plot for measurement of mobile Plk1 pool on centrosomes after Plk1 inhibition derived from N=3 independent experiments comprising n= 43, and 53 individual cells for DMSO and Plk1i, respectively. **(K)** Representative immunofluorescence images of hTERT-RPE1: Plk1-EGFP cells treated with indicated siRNAs and stained for Pericentrin (Red) and EGFP (Green). **(L)** Box and Whisker plot for measurement of Plk1 levels on centrosomes during G2 phase under the conditions indicated in **(K)** generated from N=5 independent experiments comprising n= 287: siControl, 279: siBora, 276: siCep192 and 287: siCenexin cells. Data presented as the entire range with values between first and third quartiles in boxes. '+' sign in each column represent the mean value (p values for individual comparisons indicated on graphs: Kruskal-Wallis test). Scale bars Images: 5 µm and zoomed insets: 0.5 µm.

Figure 3: (A) Live-cell time-lapse images of hTERT-RPE1: mRuby-PCNA cells treated with indicated siRNAs as they progress through S phase. **(B)** Box and whisker plot for measurement of the duration of S phase in cells after depletion of proteins indicated in **(A)**. Data derived from N=3 independent experiments comprising n= 71: siControl, 52: siCyclin A2, 68: siBora, 46: siCep192, 57: siCenexin and 62: siPlk1 cells. **(C)** Representative images of synchronised S phase RPE1 cells treated with indicated siRNAs and immunolabelled for replication forks using PCNA antibody. **(D)** Box and Whisker plot for measuring number of PCNA foci per cells as proxy for the rate of DNA replication in conditions indicated in **(C)** derived from N= 3 independent experiments comprising n= 123: siControl, 122: siBora, 126: siCep192 and 127: siCenexin cells. Data represent the entire range with

values between first and third quartiles in boxes. '+' sign in each column represent the mean value (p values for individual comparisons indicated on graphs: Kruskal-Wallis test). Scale bars: 5 µm.

Figure 4: (A) Live-cell time-lapse images of hTERT-RPE1: mRuby-PCNA cells treated with indicated siRNAs as they progress through G2 phase. **(B)** Box and whisker plot for measurement of the duration of G2 phase in cells after depletion of proteins indicated in **(A)**. Data derived from N=3 independent experiments comprising n= 83: siControl, 69: siCyclin A2, 69: siBora, 65: siCep192, 83: siCenexin and 70: siPlk1 cells. Data presented as the entire range with values between first and third quartiles in boxes. '+' sign in each column represent the mean value (p values for individual comparisons indicated on graphs: Kruskal-Wallis test). Scale bars: 5 µm.

Figure 5: (A-C) Flow cytometry-based quantification of cell cycle profile of hTERT-RPE1 (WT), hTERT-RPE1: Usp28 $^{-/-}$ and hTERT-RPE1: Usp28 $^{-/-}$ 0:0 cells revealing percentage of cells in G1 **(A)**, S **(B)** and G2 **(C)** phases derived from N=4 independent experiments with each treatment comprising around 30,000 cells. **(D)** Flow cytometry-based quantification of cell cycle profile or RPE1 cells treated with Control vs Cep192 siRNA showing percentage of cells in G1, S and G2 phases obtained from N=5 independent experiments with each treatment comprising of 30,000 cells. **(E)** Representative images of S phase hTERT-RPE1 cells expressing cellular Plk1 activity sensor and Cyclin A2-mScarlet treated with indicated siRNAs or inhibitors. **(F)** Box and Whisker plot for FRET measurement-based quantification of cellular Plk1 activity calculated from S phase cells represented in **(E)** derived from N=4 independent experiments comprising n= 203: siControl, 204: siBora, 215: siCep192, 219: siCenexin, 215: Plk1i cells. The leftmost **G2 Phase – siControl** bar shown is replica of siControl data shown in Fig 1B for side-by-side comparison purposes. **G)** Representative images of S phase hTERT-RPE1 cells expressing centrosomal Plk1 activity sensor and Cyclin A2-mScarlet treated with indicated siRNAs or inhibitors. **(H)** Box and Whisker plot for FRET measurement-based quantification of cellular Plk1 activity calculated from S phase cells represented in **(G)** derived from N=3 independent experiments comprising n= 163: siControl, 187: siBora, 187: siCep192, 184: siCenexin, 178: Plk1i cells. The leftmost **G2 Phase – siControl** bar shown is replica of siControl data

shown in Fig 1B for side-by-side comparison purposes. Data presented as the entire range with values between first and third quartiles in boxes. '+' sign in each column represent the mean value (p values for individual comparisons indicated on graphs: Kruskal-Wallis test). Scale bars, Images: 5 µm and zoomed insets: 0.5 µm.

Figure 6: (A) Schematic representation of experimental setup for investigating the role of Plk1 activators in checkpoint recovery. **(B)** Representative field images of hTERT-RPE1 cells treated with indicated siRNAs and stained for α-tubulin, Pericentrin and DAPI. **(C)** Quantification representing mitotic index after DNA damage recovery in cells under depletion different conditions shown in **(B)** obtained from N=4 independent experiments consisting of n=1136: siControl, 1398: siBora, 976: siCep192, 1359: siCenexin, 1157: siCep192 + siCenexin and 972: siPlk1 cells. **(D)** Representative field images of hTERT-RPE1 cells treated with indicated siRNAs and stained for α-tubulin, Pericentrin and DAPI. **(E)** Quantification representing mitotic index in cells without doxorubicin pulse under different depletion conditions shown in **(D)** obtained from N=3 independent experiments consisting of n=1413: siControl, 838: siBora, 827: siCep192, 1412: siCenexin, 636: siCep192 + siCenexin and 1803: siPlk1 cells. Data presented as the entire range with values between first and third quartiles in boxes. '+' sign in each column represent the mean value (p values for individual comparisons indicated on graphs: Kruskal-Wallis test). Scale bars: 5 µm.

Figure 7: (A) Representative images of G2 phase centrosomes stained with γ-tubulin (red) and Pericentrin (green) in hTERT-RPE1 cells treated with indicated siRNAs. **(B-C)** Box and Whisker plots representing the centrosomal levels of γ-tubulin **(B)** and Pericentrin **(C)** in cells represented in **(A)** as derived from N=3 independent experiments consisting of n= (168: siControl, 171: siBora, 177: siCep192, 165: siCenexin and 168: siPlk1 for γ-tubulin) and (n= 176: siControl, 170: siBora, 179: siCep192, 157: siCenexin and 183: siPlk1 for Pericentrin (green) cells. Data presented as the entire range with values between the first and third quartiles in boxes. '+' sign in each column represent the mean value (p values for individual comparisons indicated on graphs: Kruskal-Wallis test). Scale bars: 0.5 µm.

Figure 8: (A) Expansion microscopy images of centrioles in G2 phase hTERT-RPE1 (WT) and hTERT-RPE1 Cenexin $^{-/-}$ cells stained against α-tubulin and treated with indicated siRNAs to visualise centriole configuration. The arrowheads indicate the disengaged mother daughter centriole pairs. **(B)** Quantification of percentage of G2 phase hTERT-RPE1 cells with disengaged centrioles in their centrosomes (*N* = 3 independent experiments, n = 96, 98, 100 and 104 cells in siControl, siBora, siCep192 and siBora + siCep192, respectively) **(C)** Quantification of percentage of G2 phase hTERT-RPE1 Cenexin $^{-/-}$ cells with disengaged centrioles in their centrosomes (*N* = 5 independent experiments, n = 166, 149, 138 and 145 cells in siControl, siBora, siCep192 and siBora + siCep192, respectively) **(D)** Representative images of hTERT-RPE1: Centrosomal Separase activity sensor cells depicting centrosomal intensity of GFP and mCherry after indicated siRNA/drug treatments. **(E)** Box and Whisker plot for quantification of centrosomal activity of Separase in conditions depicted in **(D)** and derived from N=3 independent experiments consisting of n=142: siControl, 144: siBora, 134: siCep192, 152: siCenexin, 152: siSeparase and 147: Aphidicolin treated cells. Data presented as the entire range with values between first and third quartiles in boxes. '+' sign in each column represent the mean value (p values for individual comparisons indicated on graphs: Kruskal-Wallis test). Scale bars: 0.5 µm.

Figure S1: (A) Representative images of G2 phase hTERT-RPE1 cells expressing cellular Plk1 activity sensor and Cyclin A2-mScarlet treated with indicated siRNAs. **(B)** Box and Whisker plot for FRET measurement-based quantification of cellular Plk1 activity calculated from G2 phase cells represented in **(A)** derived from N=3 independent experiments comprising n= 120: siBora + siCep192, 135: siBora + siCenexin, 127: siBora + siCep192 + siCenexin, 124: siAurora and 121: siPlk1 cells. **(C)** Representative images of G2 phase hTERT-RPE1 cells expressing centrosomal Plk1 activity sensor and Cyclin A2-mScarlet treated with indicated siRNAs or inhibitors. **(D)** Box and Whisker plot for FRET measurement-based quantification of centrosomal Plk1 activity calculated from G2 phase cells represented in **(C)** derived from N=4 independent experiments comprising n= 181: siBora + siCep192, 187: siBora + siCenexin, 181: siBora + siCep192 + siCenexin, 182: siAurora

and 182: siPlk1 cells. **(E-G)** Western Blot confirming the depletion of indicated proteins after indicated siRNA treatments. Data represent the entire range with values between first and third quartiles in boxes. '+' sign in each column represent the mean value (p values for individual comparisons indicated on graphs: Kruskal-Wallis test). Scale bars = 5 µm.

Figure S2: (A-D) Representative time stamp images and quantifications from FRAP movies from G2 phase Plk1-EGFP tagged hTERT-RPE1 cells treated with DMSO **(A**: quantification of Plk1 recovery on centrosomes in **(B))** and Plk1i (**(C**: quantification of Plk1 recovery on centrosomes in **(D))**. Data obtained from N=3 independent experiments consisting of n=43 and 53 DMSO and Plk1i treated cells, respectively. **(E)** Representative immunofluorescence images of hTERT-RPE1: Plk1-EGFP cells treated with indicated siRNAs and stained for Pericentrin (Red) and EGFP (Green). **(F)** Box and Whisker plot for measurement of Plk1 levels on centrosomes during G2 phase under the conditions indicated in **(E)** generated from N=5 independent experiments comprising n= 276: siBora + siCep192, 287: siCep192 + siCenexin, 286: Bora + siCenexin and 282: siBora + siCep192 + siCenexin cells. Data presented as the entire range with values between first and third quartiles in boxes. '+' sign in each column represent the mean value (p values for individual comparisons indicated on graphs: Kruskal-Wallis test). Scale bars Images: 2 µm and zoomed insets: 0.5 µm.

Figure S3 (A) Live-cell time-lapse images of hTERT-RPE1: mRuby-PCNA cells treated with indicated siRNA combinations as they progress through S phase. **(B)** Box and whisker plot for measurement of the duration of S phase in cells after depletion of proteins indicated in **(A)**. Data derived from N=3 independent experiments comprising n= 45: siBora + Cep192, 52: siCep192 + siCenexin, 57: siBora + siCenexin and 51: siBora + siCep192 + siCenexin cells. **(C)** Live-cell time-lapse images of hTERT-RPE1: mRuby-PCNA cells treated with indicated siRNA combinations as they progress through G2 phase. **(D)** Box and whisker plot for measurement of the duration of S phase in cells after depletion of proteins indicated in **(A)**. Data derived from N=3 independent experiments comprising n= 82: siBora + Cep192, 56: siCep192 + siCenexin, 64: siBora + siCenexin and 71: siBora + siCep192 + siCenexin cells. Data presented as the entire range with values between first and third

quartiles in boxes. '+' sign in each column represent the mean value (p values for individual comparisons indicated on graphs: Kruskal-Wallis test). Scale bars: 5 µm.

Figure S4 (A) Representative images of interphase and metaphase hTERT-RPE1: Usp28 $^{-/-}$ and hTERT-RPE1: Usp28 $^{-/-}$ 0:0 cells stained for centrioles with Centrin (green) confirming absence of centrosomes. **(B)** Box and Whisker plot depicting the number of centrioles present in hTERT-RPE1: Usp28 $^{-/-}$ and hTERT-RPE1: Usp28 $^{-/-}$ 0:0 cells calculated from N=3 independent experiments with a total of n= 47 cells in each case. Data presented as the entire range with values between first and third quartiles in boxes. '+' sign in each column represent the mean value (p values for the comparisons indicated on graph: Student's t-test). Scale bars: 5 µm.

Figure S5 (A) Representative images of synchronised and doxorubicin pulsed hTERT-RPE1 cells treated with indicated siRNA combinations and stained for γ-H2AX (green) to confirm induction of DNA damage after doxorubicin pulse. **(B)** Representative field images of hTERT-RPE1 cells treated with indicated siRNAs and stained for α-tubulin, Pericentrin and DAPI. **(C)** Quantification representing mitotic index in cells without doxorubicin pulse under indicated depletion conditions shown in **(B)** obtained from N=3 independent experiments consisting of n=591: siBora + siCep192, 955: siBora + siCenexin and 637: siBora + siCep192 + siCenexin cells. Data presented as the entire range with values between first and third quartiles in boxes. '+' sign in each column represent the mean value (p values for individual comparisons indicated on graphs: Kruskal-Wallis test). Scale bars: 5 µm.

Figure S6: (A) Representative images of G2 phase centrosomes stained with γ-tubulin (red) and Pericentrin (green) in hTERT-RPE1 cells treated with indicated siRNA combinations. **(B-C)** Box and Whisker plots representing the centrosomal levels of γ-tubulin **(B)** and Pericentrin **(C)** in cells represented in **(A)** as derived from N=3 independent experiments consisting of n= (138: siBora + siCep192, 164: siCep192 + siCenexin, 181: siCenexin + siBora and 167: siBora + siCep192 + siCenexin for γ-tubulin) and (n= 136: siBora + siCep192, 167: siCep192 + siCenexin, 181: siCenexin + siBora and 170: siBora + siCep192 + siCenexin for Pericentrin (green) cells. Data presented as the

entire range with values between the first and third quartiles in boxes. '+' sign in each column represent the mean value (p values for individual comparisons indicated on graphs: Kruskal-Wallis test). Scale bars: 0.5 µm.

Figure S7 (A) Representative images of hTERT-RPE1 cells treated with indicated siRNA/drugs and stained for indicated DNA damage marker proteins. **(B)** Box and Whisker plots depicting the size of γ-H2AX nuclear puncta shown in **(A)** from N=3 independent experiments with n= 186: siControl, 184: siBora, 186: siCep192, 187: siCenexin and 166: Aphidicolin treated cells. **(C)** Box and Whisker plots depicting the size of 53BP1 nuclear puncta shown in **(A)** from N=3 independent experiments with n= 228: siControl, 219: siBora, 169: siCep192, 223: siCenexin and 227: Aphidicolin treated cells. Data presented as the entire range with values between the first and third quartiles in boxes. '+' sign in each column represent the mean value (p values for individual comparisons indicated on graphs: Kruskal-Wallis test). Scale bars: 0.5 µm.

Supplementary Movies

Movie 1: FRAP recordings of hTERT-RPE1 expressing endogenously tagged Plk1-EGFP and treated with siControl. Every image was captured at an interval of 5s. The movie is shown at 3 frames per second (fps). Scale bars, 5 µm.

Movie 2: FRAP recordings of hTERT-RPE1 expressing endogenously tagged Plk1-EGFP and treated with siCep192. Every image was captured at an interval of 5s. The movie is shown at 3 frames per second (fps). Scale bars, 5 µm.

Movie 3: FRAP recordings of hTERT-RPE1 expressing endogenously tagged Plk1-EGFP and treated with siCenexin. Every image was captured at an interval of 5s. The movie is shown at 3 frames per second (fps). Scale bars, 5 µm.

Movie 4: FRAP recordings of hTERT-RPE1 expressing endogenously tagged Plk1-EGFP and co-treated with siCep192 and siCenexin. Every image was captured at an interval of 5s. The movie is shown at 3 frames per second (fps). Scale bars, 5 µm.

Movie 5: FRAP recordings of hTERT-RPE1 expressing endogenously tagged Plk1-EGFP and treated with DMSO/Control. Every image was captured at an interval of 4s. The movie is shown at 3 frames per second (fps). Scale bars, 5 µm.

Movie 6: FRAP recordings of hTERT-RPE1 expressing endogenously tagged Plk1-EGFP and treated with Plk1i(BI2536). Every image was captured at an interval of 5s. The movie is shown at 3 frames per second (fps). Scale bars, 5 µm.

Movie 7: Live-cell imaging of hTERT-RPE1 expressing endogenously tagged mRuby-PCNA and treated with siControl progressing through S phase. Every image was captured at an interval of 10 m. The movie is shown at 5 frames per second (fps). Scale bars, 5 µm.

Movie 8: Live-cell imaging of hTERT-RPE1 expressing endogenously tagged mRuby-PCNA and treated with siControl progressing through G2 phase. Every image was captured at an interval of 10 m. The movie is shown at 5 frames per second (fps). Scale bars, 5 µm.

Movie 9: Live-cell imaging of hTERT-RPE1 expressing endogenously tagged mRuby-PCNA and treated with siCyclin A2 progressing through S phase. Every image was captured at an interval of 10 m. The movie is shown at 5 frames per second (fps). Scale bars, 5 µm.

Movie 10: Live-cell imaging of hTERT-RPE1 expressing endogenously tagged mRuby-PCNA and treated with siCyclin A2 progressing through G2 phase. Every image was captured at an interval of 10 m. The movie is shown at 5 frames per second (fps). Scale bars, 5 µm.

Movie 11: Live-cell imaging of hTERT-RPE1 expressing endogenously tagged mRuby-PCNA and treated with siBora progressing through S phase. Every image was captured at an interval of 10 m. The movie is shown at 5 frames per second (fps). Scale bars, 5 µm.

Movie 12: Live-cell imaging of hTERT-RPE1 expressing endogenously tagged mRuby-PCNA and treated with siCep192 progressing through S phase. Every image was captured at an interval of 10 m. The movie is shown at 5 frames per second (fps). Scale bars, 5 µm.

Movie 13: Live-cell imaging of hTERT-RPE1 expressing endogenously tagged mRuby-PCNA and treated with siCenexin progressing through S phase. Every image was captured at an interval of 10 m. The movie is shown at 5 frames per second (fps). Scale bars, 5 µm.

Movie 14: Live-cell imaging of hTERT-RPE1 expressing endogenously tagged mRuby-PCNA and co-treated with siBora and Cep192 progressing through S phase. Every image was captured at an interval of 10 m. The movie is shown at 5 frames per second (fps). Scale bars, 5 µm.

Movie 15: Live-cell imaging of hTERT-RPE1 expressing endogenously tagged mRuby-PCNA and co-treated with siCep192 and siCenexin progressing through S phase. Every image was captured at an interval of 10 m. The movie is shown at 5 frames per second (fps). Scale bars, 5 µm.

Movie 16: Live-cell imaging of hTERT-RPE1 expressing endogenously tagged mRuby-PCNA and co-treated with siBora and siCenexin progressing through S phase. Every image was captured at an interval of 10 m. The movie is shown at 5 frames per second (fps). Scale bars, 5 µm.

Movie 17: Live-cell imaging of hTERT-RPE1 expressing endogenously tagged mRuby-PCNA and co-treated with siBora, siCep192 and siCenexin progressing through S phase. Every image was captured at an interval of 10 m. The movie is shown at 5 frames per second (fps). Scale bars, 5 µm.

Movie 18: Live-cell imaging of hTERT-RPE1 expressing endogenously tagged mRuby-PCNA and treated with siPlk1 progressing through S phase. Every image was captured at an interval of 10 m. The movie is shown at 5 frames per second (fps). Scale bars, 5 µm.

Movie 19: Live-cell imaging of hTERT-RPE1 expressing endogenously tagged mRuby-PCNA and treated with siBora progressing through G2 phase. Every image was captured at an interval of 10 m. The movie is shown at 5 frames per second (fps). Scale bars, 5 µm.

Movie 20: Live-cell imaging of hTERT-RPE1 expressing endogenously tagged mRuby-PCNA and treated with siCep192 progressing through G2 phase. Every image was captured at an interval of 10 m. The movie is shown at 5 frames per second (fps). Scale bars, 5 µm.

Movie 21: Live-cell imaging of hTERT-RPE1 expressing endogenously tagged mRuby-PCNA and treated with siCenexin progressing through G2 phase. Every image was captured at an interval of 10 m. The movie is shown at 5 frames per second (fps). Scale bars, 5 µm.

Movie 22: Live-cell imaging of hTERT-RPE1 expressing endogenously tagged mRuby-PCNA and co-treated with siBora and Cep192 progressing through G2 phase. Every image was captured at an interval of 10 m. The movie is shown at 5 frames per second (fps). Scale bars, 5 µm.

Movie 23: Live-cell imaging of hTERT-RPE1 expressing endogenously tagged mRuby-PCNA and co-treated with siCep192 and siCenexin progressing through G2 phase. Every image was captured at an interval of 10 m. The movie is shown at 5 frames per second (fps). Scale bars, 5 µm.

Movie 24: Live-cell imaging of hTERT-RPE1 expressing endogenously tagged mRuby-PCNA and co-treated with siBora and siCenexin progressing through G2 phase. Every image was captured at an interval of 10 m. The movie is shown at 5 frames per second (fps). Scale bars, 5 µm.

Movie 25: Live-cell imaging of hTERT-RPE1 expressing endogenously tagged mRuby-PCNA and co-treated with siBora, siCep192 and siCenexin progressing through G2 phase. Every image was captured at an interval of 10 m. The movie is shown at 5 frames per second (fps). Scale bars, 5 µm.

Movie 26: Live-cell imaging of hTERT-RPE1 expressing endogenously tagged mRuby-PCNA and treated with siPlk1 progressing through G2 phase. Every image was captured at an interval of 10 m. The movie is shown at 5 frames per second (fps). Scale bars, 5 µm.

References

1. Zitouni, S., Nabais, C., Jana, S.C., Guerrero, A. & Bettencourt-Dias, M. Polo-like kinases: structural variations lead to multiple functions. *Nat Rev Mol Cell Biol* **15**, 433–452 (2014).
2. Gheghiani, L., Loew, D., Lombard, B., Mansfeld, J. & Gavet, O. PLK1 Activation in Late G2 Sets Up Commitment to Mitosis. *Cell Rep* **19**, 2060–2073 (2017).
3. Nakajima, H., Toyoshima-Morimoto, F., Taniguchi, E. & Nishida, E. Identification of a consensus motif for Plk (Polo-like kinase) phosphorylation reveals Myt1 as a Plk1 substrate. *J Biol Chem* **278**, 25277–25280 (2003).
4. Watanabe, N. *et al.* Cyclin-dependent kinase (CDK) phosphorylation destabilizes somatic Wee1 via multiple pathways. *Proc Natl Acad Sci U S A* **102**, 11663–11668 (2005).
5. Bailey, L.J. *et al.* PLK1 regulates the PrimPol damage tolerance pathway during the cell cycle. *Sci Adv* **7**, eabh1004 (2021).
6. Bruinsma, W., Macurek, L., Freire, R., Lindqvist, A. & Medema, R.H. Bora and Aurora-A continue to activate Plk1 in mitosis. *J Cell Sci* **127**, 801–811 (2014).
7. van Vugt, M.A., Bras, A. & Medema, R.H. Polo-like kinase-1 controls recovery from a G2 DNA damage-induced arrest in mammalian cells. *Mol Cell* **15**, 799–811 (2004).
8. Barbosa, J. *et al.* Polo regulates Spindly to prevent premature stabilization of kinetochore-microtubule attachments. *EMBO J* **39**, e100789 (2020).
9. Park, C.H. *et al.* Mammalian Polo-like kinase 1 (Plk1) promotes proper chromosome segregation by phosphorylating and delocalizing the PBIP1.CENP-Q complex from kinetochores. *J Biol Chem* **290**, 8569–8581 (2015).
10. Li, H. *et al.* Phosphorylation of CLIP-170 by Plk1 and CK2 promotes timely formation of kinetochore-microtubule attachments. *EMBO J* **29**, 2953–2965 (2010).
11. Elia, A.E., Cantley, L.C. & Yaffe, M.B. Proteomic screen finds pSer/pThr-binding domain localizing Plk1 to mitotic substrates. *Science* **299**, 1228–1231 (2003).
12. Elia, A.E. *et al.* The molecular basis for phosphodependent substrate targeting and regulation of Plks by the Polo-box domain. *Cell* **115**, 83–95 (2003).
13. Xu, J., Shen, C., Wang, T. & Quan, J. Structural basis for the inhibition of Polo-like kinase 1. *Nat Struct Mol Biol* **20**, 1047–1053 (2013).
14. Chapagai, D., Strebhardt, K., Wyatt, M.D. & McInnes, C. Structural regulation of PLK1 activity: implications for cell cycle function and drug discovery. *Cancer Gene Ther* **32**, 608–621 (2025).
15. Bruinsma, W. *et al.* Spatial Separation of Plk1 Phosphorylation and Activity. *Front Oncol* **5**, 132 (2015).
16. Kachaner, D. *et al.* Coupling of Polo kinase activation to nuclear localization by a bifunctional NLS is required during mitotic entry. *Nat Commun* **8**, 1701 (2017).
17. Silva Cascales, H. *et al.* Cyclin A2 localises in the cytoplasm at the S/G2 transition to activate PLK1. *Life Sci Alliance* **4** (2021).
18. Cheng, K.Y., Lowe, E.D., Sinclair, J., Nigg, E.A. & Johnson, L.N. The crystal structure of the human polo-like kinase-1 polo box domain and its phospho-peptide complex. *EMBO J* **22**, 5757–5768 (2003).
19. Esposito Verza, A. *et al.* Molecular requirements for PLK1 activation by T-loop phosphorylation. *bioRxiv*, 2025.2007.2025.666769 (2025).
20. Pillan, A. *et al.* Molecular basis for the activation of Aurora A and Plk1 kinases during mitotic entry. *bioRxiv*, 2025.2007.2025.666770 (2025).
21. Seki, A., Coppinger, J.A., Jang, C.Y., Yates, J.R. & Fang, G. Bora and the kinase Aurora a cooperatively activate the kinase Plk1 and control mitotic entry. *Science* **320**, 1655–1658 (2008).
22. Macurek, L. *et al.* Polo-like kinase-1 is activated by aurora A to promote checkpoint recovery. *Nature* **455**, 119–123 (2008).

23. Tavernier, N. *et al.* Bora phosphorylation substitutes in trans for T-loop phosphorylation in Aurora A to promote mitotic entry. *Nat Commun* **12**, 1899 (2021).
24. Thomas, Y. *et al.* Cdk1 Phosphorylates SPAT-1/Bora to Promote Plk1 Activation in C. elegans and Human Cells. *Cell Rep* **15**, 510–518 (2016).
25. Vigneron, S. *et al.* Cyclin A-cdk1-Dependent Phosphorylation of Bora Is the Triggering Factor Promoting Mitotic Entry. *Dev Cell* **45**, 637–650 e637 (2018).
26. Joukov, V., Walter, J.C. & De Nicolo, A. The Cep192-organized aurora A-Plk1 cascade is essential for centrosome cycle and bipolar spindle assembly. *Mol Cell* **55**, 578–591 (2014).
27. Joukov, V., De Nicolo, A., Rodriguez, A., Walter, J.C. & Livingston, D.M. Centrosomal protein of 192 kDa (Cep192) promotes centrosome-driven spindle assembly by engaging in organelle-specific Aurora A activation. *Proc Natl Acad Sci U S A* **107**, 21022–21027 (2010).
28. Aljiboury, A. *et al.* Pericentriolar matrix (PCM) integrity relies on cenexin and polo-like kinase (PLK)1. *Mol Biol Cell* **33**, br14 (2022).
29. Colicino, E.G. *et al.* Chromosome misalignment is associated with PLK1 activity at cenexin-positive mitotic centrosomes. *Mol Biol Cell* **30**, 1598–1609 (2019).
30. Thomas, A. & Meraldi, P. Centrosome age breaks spindle size symmetry even in cells thought to divide symmetrically. *J Cell Biol* **223** (2024).
31. Golsteyn, R.M., Mundt, K.E., Fry, A.M. & Nigg, E.A. Cell cycle regulation of the activity and subcellular localization of Plk1, a human protein kinase implicated in mitotic spindle function. *J Cell Biol* **129**, 1617–1628 (1995).
32. Liu, D., Davydenko, O. & Lampson, M.A. Polo-like kinase-1 regulates kinetochore-microtubule dynamics and spindle checkpoint silencing. *J Cell Biol* **198**, 491–499 (2012).
33. Colicino, E.G. *et al.* Gravin regulates centrosome function through PLK1. *Mol Biol Cell* **29**, 532–541 (2018).
34. Steegmaier, M. *et al.* BI 2536, a potent and selective inhibitor of polo-like kinase 1, inhibits tumor growth in vivo. *Curr Biol* **17**, 316–322 (2007).
35. Ciardo, D. *et al.* Polo-like kinase 1 (Plk1) is a positive regulator of DNA replication in the Xenopus in vitro system. *Cell Cycle* **19**, 1817–1832 (2020).
36. Ciardo, D. *et al.* Polo-like kinase 1 (Plk1) regulates DNA replication origin firing and interacts with Rif1 in Xenopus. *Nucleic Acids Res* **49**, 9851–9869 (2021).
37. Haccard, O. *et al.* Rif1 restrains the rate of replication origin firing in Xenopus laevis. *Commun Biol* **6**, 788 (2023).
38. Toogood, P.L. *et al.* Discovery of a potent and selective inhibitor of cyclin-dependent kinase 4/6. *J Med Chem* **48**, 2388–2406 (2005).
39. Leonhardt, H. *et al.* Dynamics of DNA replication factories in living cells. *J Cell Biol* **149**, 271–280 (2000).
40. Kim, T.S. *et al.* Hierarchical recruitment of Plk4 and regulation of centriole biogenesis by two centrosomal scaffolds, Cep192 and Cep152. *Proc Natl Acad Sci U S A* **110**, E4849–4857 (2013).
41. Sonnen, K.F., Gabryjonczyk, A.M., Anselm, E., Stierhof, Y.D. & Nigg, E.A. Human Cep192 and Cep152 cooperate in Plk4 recruitment and centriole duplication. *J Cell Sci* **126**, 3223–3233 (2013).
42. Wong, Y.L. *et al.* Cell biology. Reversible centriole depletion with an inhibitor of Polo-like kinase 4. *Science* **348**, 1155–1160 (2015).
43. Meitinger, F. *et al.* 53BP1 and USP28 mediate p53 activation and G1 arrest after centrosome loss or extended mitotic duration. *J Cell Biol* **214**, 155–166 (2016).
44. Burigotto, M. *et al.* PLK1 promotes the mitotic surveillance pathway by controlling cytosolic 53BP1 availability. *EMBO Rep* **24**, e57234 (2023).
45. van Vugt, M.A. *et al.* A mitotic phosphorylation feedback network connects Cdk1, Plk1, 53BP1, and Chk2 to inactivate the G(2)/M DNA damage checkpoint. *PLoS Biol* **8**, e1000287 (2010).

46. Jaiswal, H. *et al.* ATM/Wip1 activities at chromatin control Plk1 re-activation to determine G2 checkpoint duration. *EMBO J* **36**, 2161–2176 (2017).
47. Lemmens, B. *et al.* DNA Replication Determines Timing of Mitosis by Restricting CDK1 and PLK1 Activation. *Mol Cell* **71**, 117–128 e113 (2018).
48. Blanco-Ameijeiras, J., Lozano-Fernandez, P. & Marti, E. Centrosome maturation - in tune with the cell cycle. *J Cell Sci* **135** (2022).
49. Kim, J., Kim, J. & Rhee, K. PCNT is critical for the association and conversion of centrioles to centrosomes during mitosis. *J Cell Sci* **132** (2019).
50. Lee, K. & Rhee, K. PLK1 phosphorylation of pericentrin initiates centrosome maturation at the onset of mitosis. *J Cell Biol* **195**, 1093–1101 (2011).
51. Ohta, M. *et al.* Polo-like kinase 1 independently controls microtubule-nucleating capacity and size of the centrosome. *J Cell Biol* **220** (2021).
52. Kim, J., Lee, K. & Rhee, K. PLK1 regulation of PCNT cleavage ensures fidelity of centriole separation during mitotic exit. *Nat Commun* **6**, 10076 (2015).
53. Kong, D. *et al.* Centriole maturation requires regulated Plk1 activity during two consecutive cell cycles. *J Cell Biol* **206**, 855–865 (2014).
54. Shukla, A., Kong, D., Sharma, M., Magidson, V. & Loncarek, J. Plk1 relieves centriole block to reduplication by promoting daughter centriole maturation. *Nat Commun* **6**, 8077 (2015).
55. Dwivedi, D., Harry, D. & Meraldi, P. Mild replication stress causes premature centriole disengagement via a sub-critical Plk1 activity under the control of ATR-Chk1. *Nat Commun* **14**, 6088 (2023).
56. Dwivedi, D. & Meraldi, P. Balancing Plk1 activity levels: The secret of synchrony between the cell and the centrosome cycle. *Bioessays* **46**, e2400048 (2024).
57. Lee, K. & Rhee, K. Separase-dependent cleavage of pericentrin B is necessary and sufficient for centriole disengagement during mitosis. *Cell Cycle* **11**, 2476–2485 (2012).
58. Matsuo, K. *et al.* Kendrin is a novel substrate for separase involved in the licensing of centriole duplication. *Curr Biol* **22**, 915–921 (2012).
59. Tsou, M.F. *et al.* Polo kinase and separase regulate the mitotic licensing of centriole duplication in human cells. *Dev Cell* **17**, 344–354 (2009).
60. Agircan, F.G. & Schiebel, E. Sensors at centrosomes reveal determinants of local separase activity. *PLoS Genet* **10**, e1004672 (2014).
61. Kang, Y.H. *et al.* Self-regulated Plk1 recruitment to kinetochores by the Plk1-PBIP1 interaction is critical for proper chromosome segregation. *Mol Cell* **24**, 409–422 (2006).
62. Wong, S.S. *et al.* Centrioles generate a local pulse of Polo/PLK1 activity to initiate mitotic centrosome assembly. *EMBO J* **41**, e110891 (2022).
63. Mahen, R., Jeyasekharan, A.D., Barry, N.P. & Venkitaraman, A.R. Continuous polo-like kinase 1 activity regulates diffusion to maintain centrosome self-organization during mitosis. *Proc Natl Acad Sci U S A* **108**, 9310–9315 (2011).
64. Meng, L. *et al.* Bimodal Interaction of Mammalian Polo-Like Kinase 1 and a Centrosomal Scaffold, Cep192, in the Regulation of Bipolar Spindle Formation. *Mol Cell Biol* **35**, 2626–2640 (2015).
65. Li, W. *et al.* A methylation-phosphorylation switch determines Plk1 kinase activity and function in DNA damage repair. *Sci Adv* **5**, eaau7566 (2019).
66. Bruinsma, W. *et al.* Inhibition of Polo-like kinase 1 during the DNA damage response is mediated through loss of Aurora A recruitment by Bora. *Oncogene* **36**, 1840–1848 (2017).
67. Hirota, T. *et al.* Aurora-A and an interacting activator, the LIM protein Ajuba, are required for mitotic commitment in human cells. *Cell* **114**, 585–598 (2003).
68. Conduit, P.T. *et al.* The centrosome-specific phosphorylation of Cnn by Polo/Plk1 drives Cnn scaffold assembly and centrosome maturation. *Dev Cell* **28**, 659–669 (2014).
69. Hu, L. *et al.* The conserved Spd-2/CEP192 domain adopts a unique protein fold to promote centrosome scaffold assembly. *Sci Adv* **11**, eadr5744 (2025).

70. Zhu, F. *et al.* The mammalian SPD-2 ortholog Cep192 regulates centrosome biogenesis. *Curr Biol* **18**, 136–141 (2008).
71. Holder, J. *et al.* CEP192 localises mitotic Aurora-A activity by priming its interaction with TPX2. *EMBO J* **43**, 5381–5420 (2024).
72. Wong, S.S., Wainman, A., Saurya, S. & Raff, J.W. Regulation of centrosome size by the cell-cycle oscillator in Drosophila embryos. *EMBO J* **43**, 414–436 (2024).
73. Chan, E.H., Santamaria, A., Sillje, H.H. & Nigg, E.A. Plk1 regulates mitotic Aurora A function through betaTrCP-dependent degradation of hBora. *Chromosoma* **117**, 457–469 (2008).
74. Seki, A. *et al.* Plk1- and beta-TrCP-dependent degradation of Bora controls mitotic progression. *J Cell Biol* **181**, 65–78 (2008).
75. Mazo, G., Soplop, N., Wang, W.J., Uryu, K. & Tsou, M.F. Spatial Control of Primary Ciliogenesis by Subdistal Appendages Alters Sensation-Associated Properties of Cilia. *Dev Cell* **39**, 424–437 (2016).
76. Barr, A.R. *et al.* DNA damage during S-phase mediates the proliferation-quiescence decision in the subsequent G1 via p21 expression. *Nat Commun* **8**, 14728 (2017).
77. Waizenegger, I., Gimenez-Abian, J.F., Wernic, D. & Peters, J.M. Regulation of human separase by securin binding and autocleavage. *Curr Biol* **12**, 1368–1378 (2002).
78. Guerreiro, A. & Meraldi, P. AA344 and AA345 antibodies recognize the microtubule network in human cells by immunofluorescence. *Antibody Reports* **2**, e17 (2019).

Figure 1. Dwivedi et al.

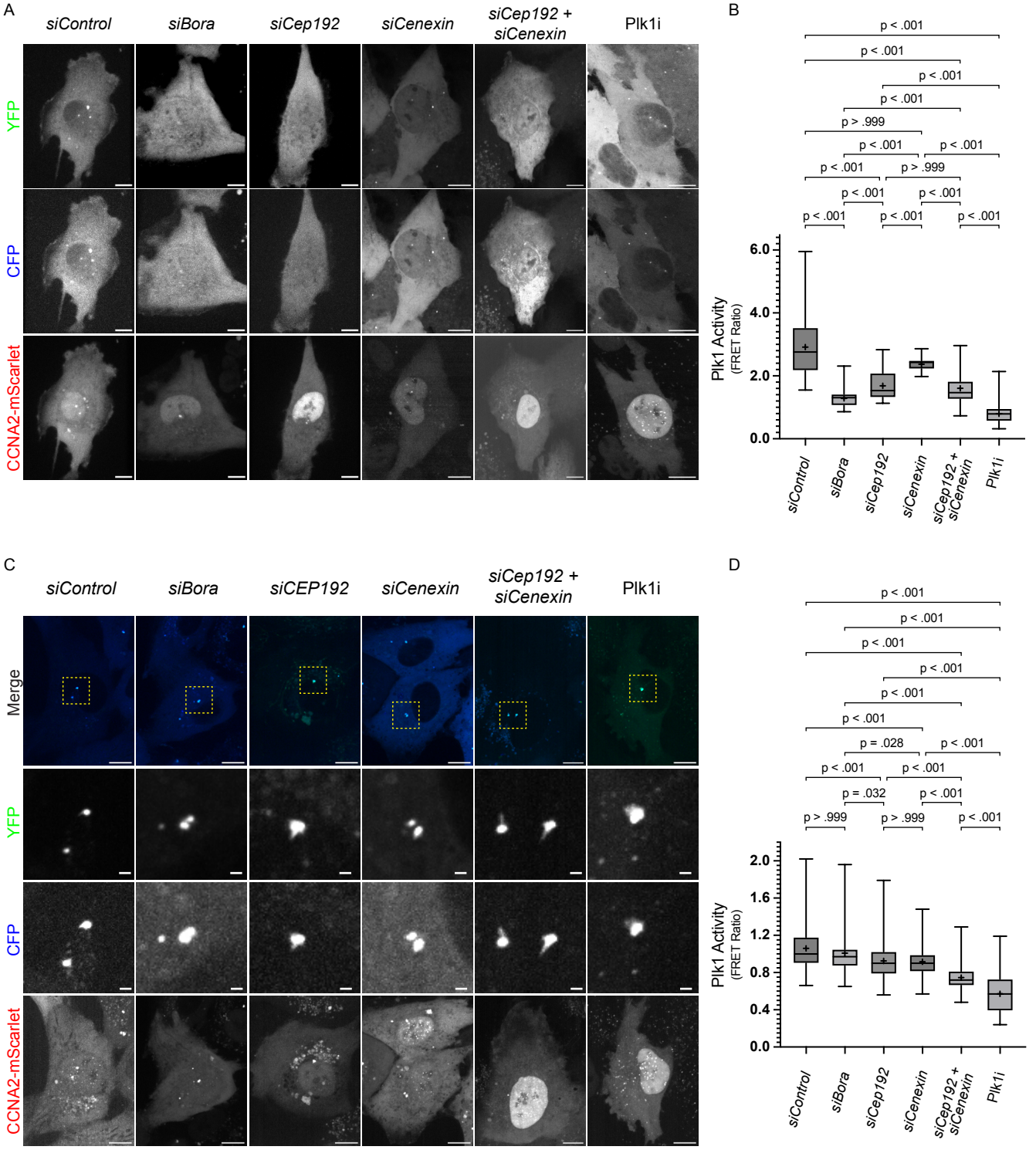

Figure 2. Dwivedi et al.

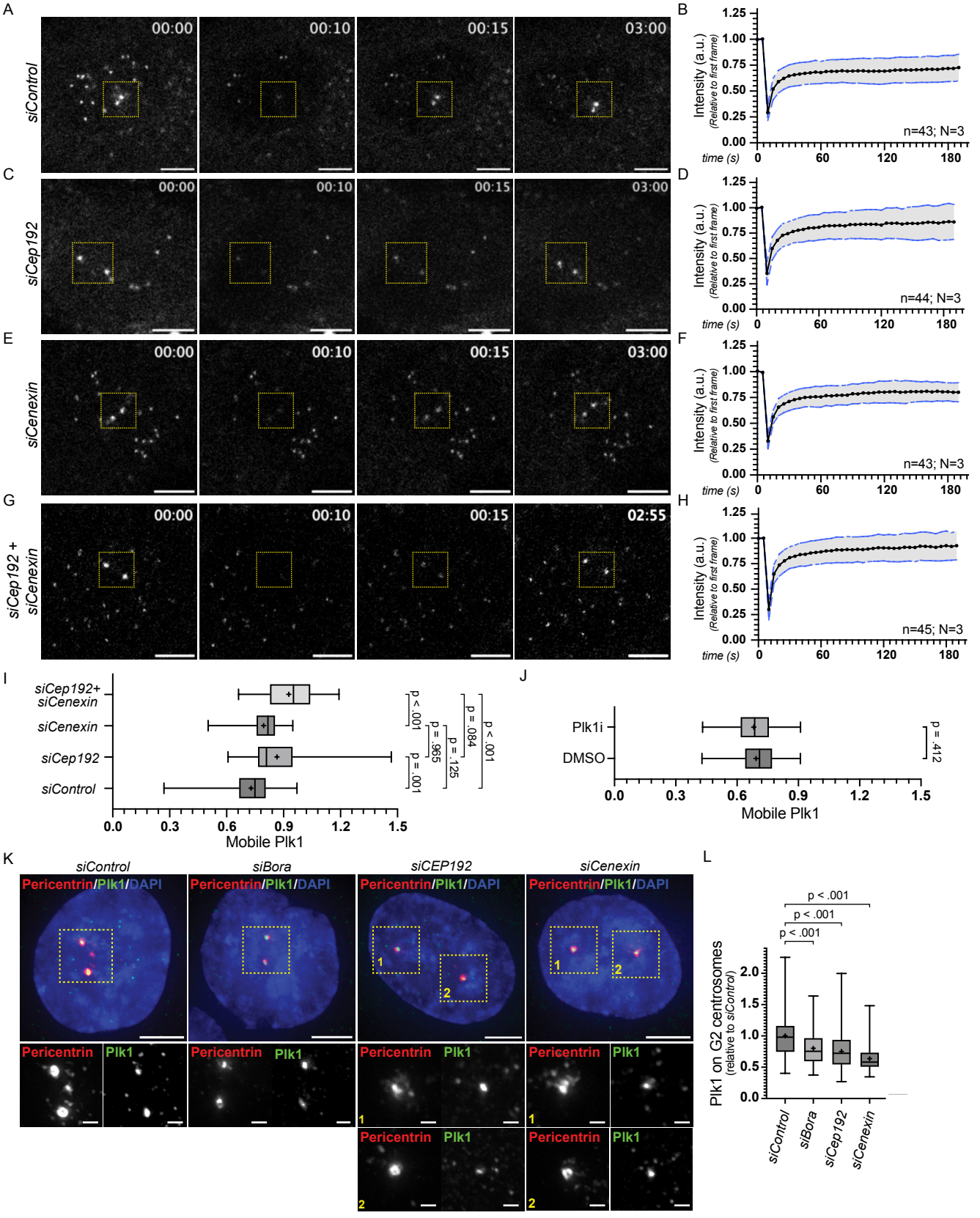

Figure 3. Dwivedi et al.

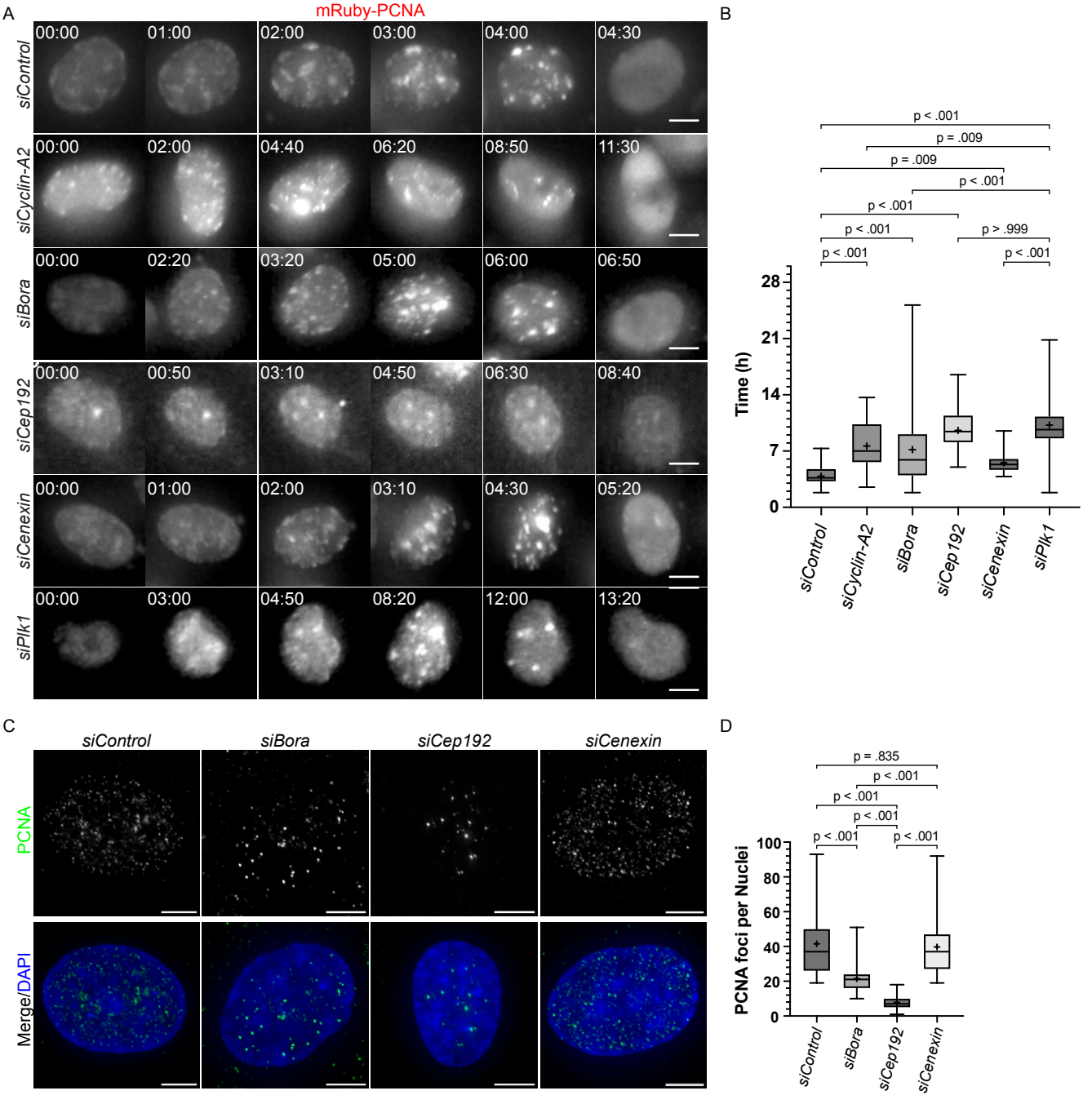

Figure 4. Dwivedi et al.

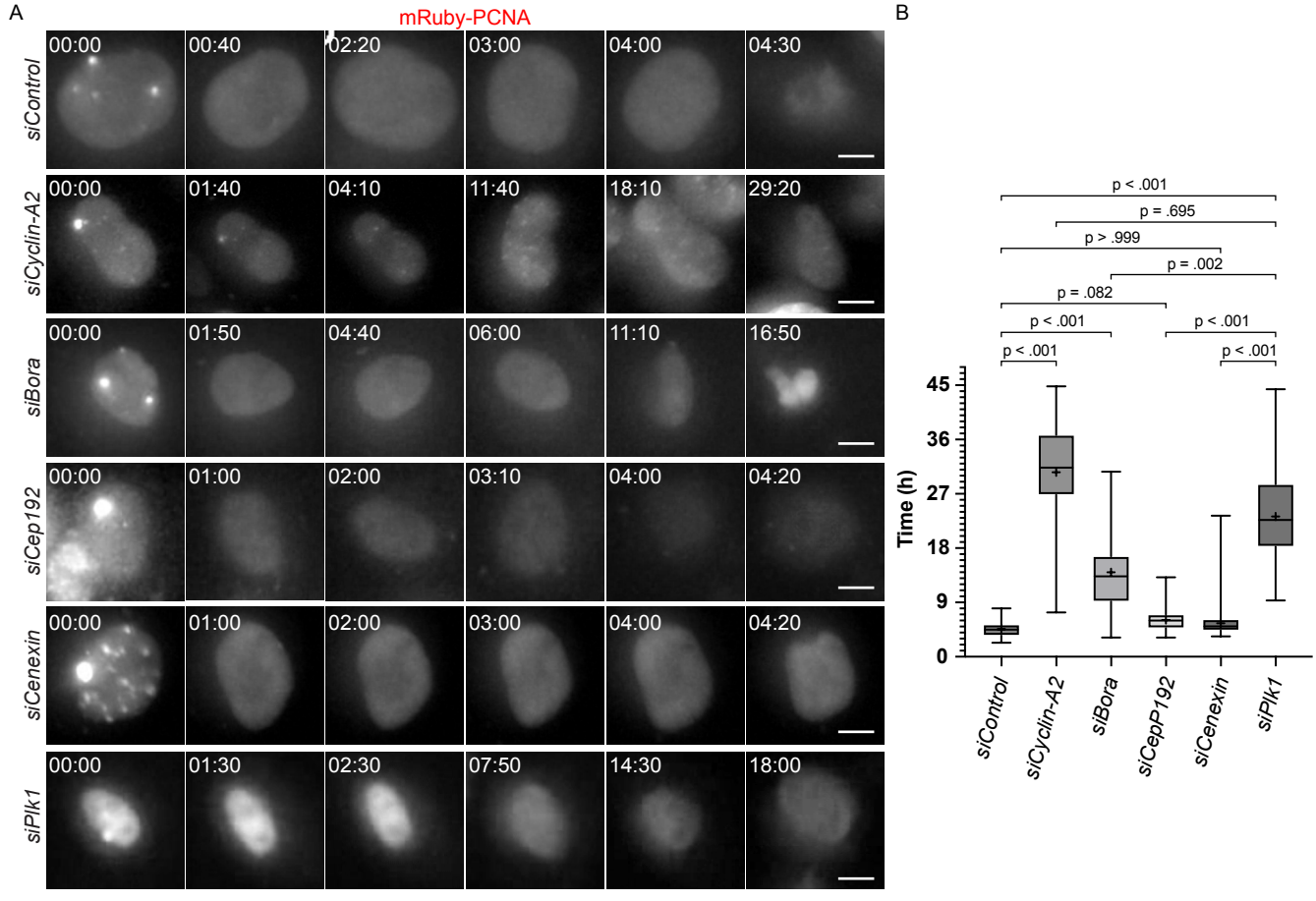

Figure 5. Dwivedi et al.

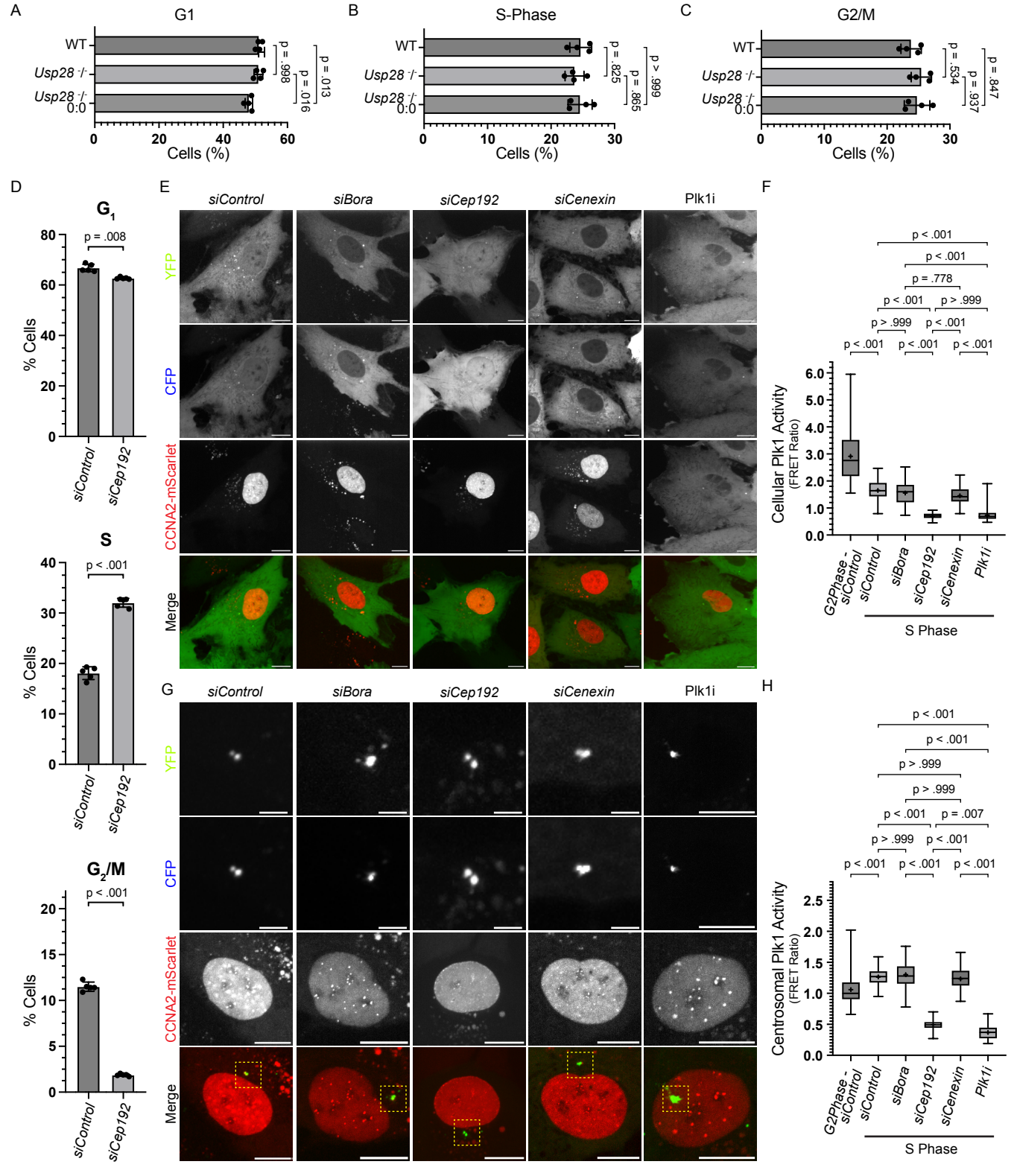

Figure 6. Dwivedi et al.

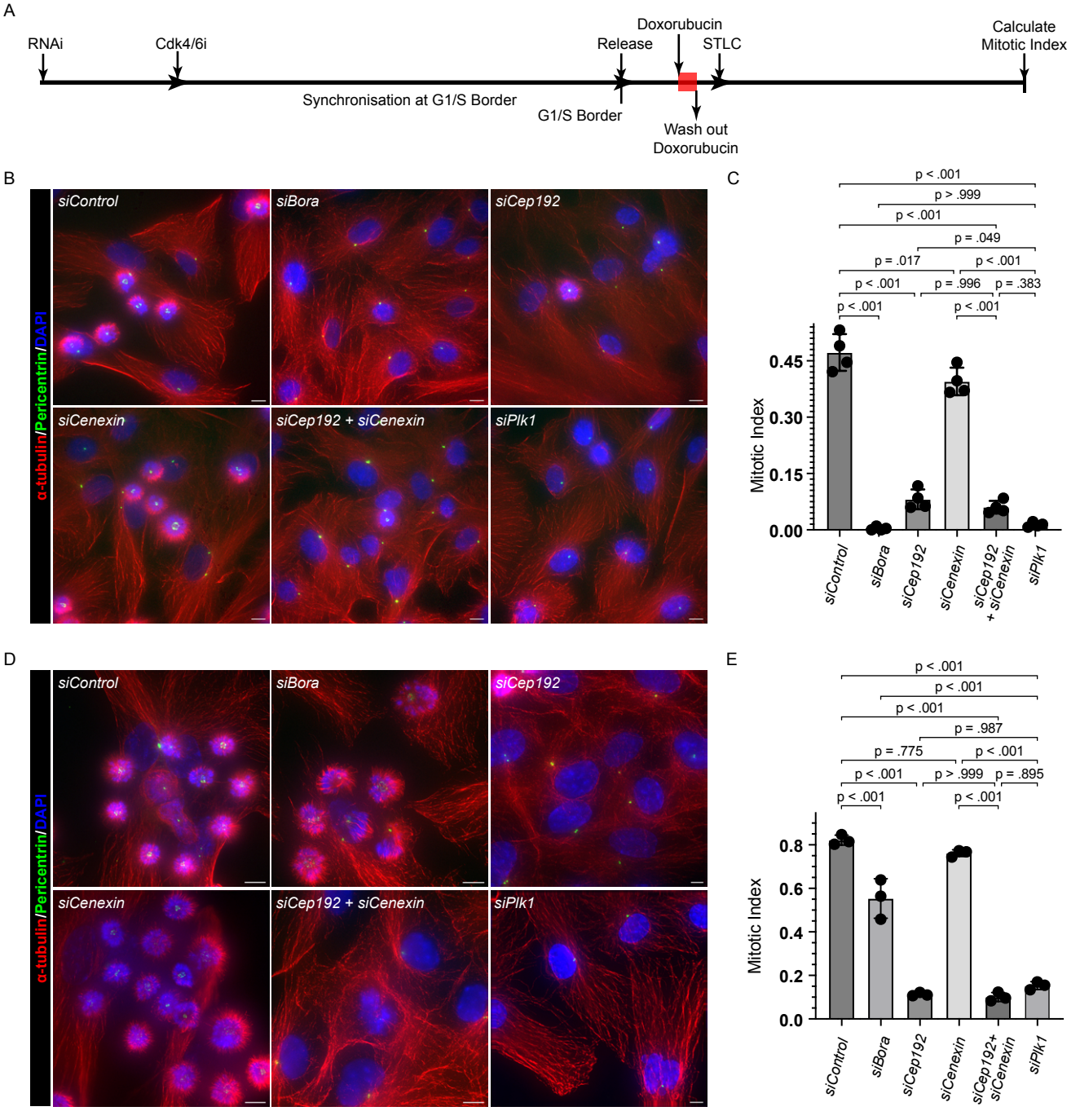

Figure 7. Dwivedi et al.

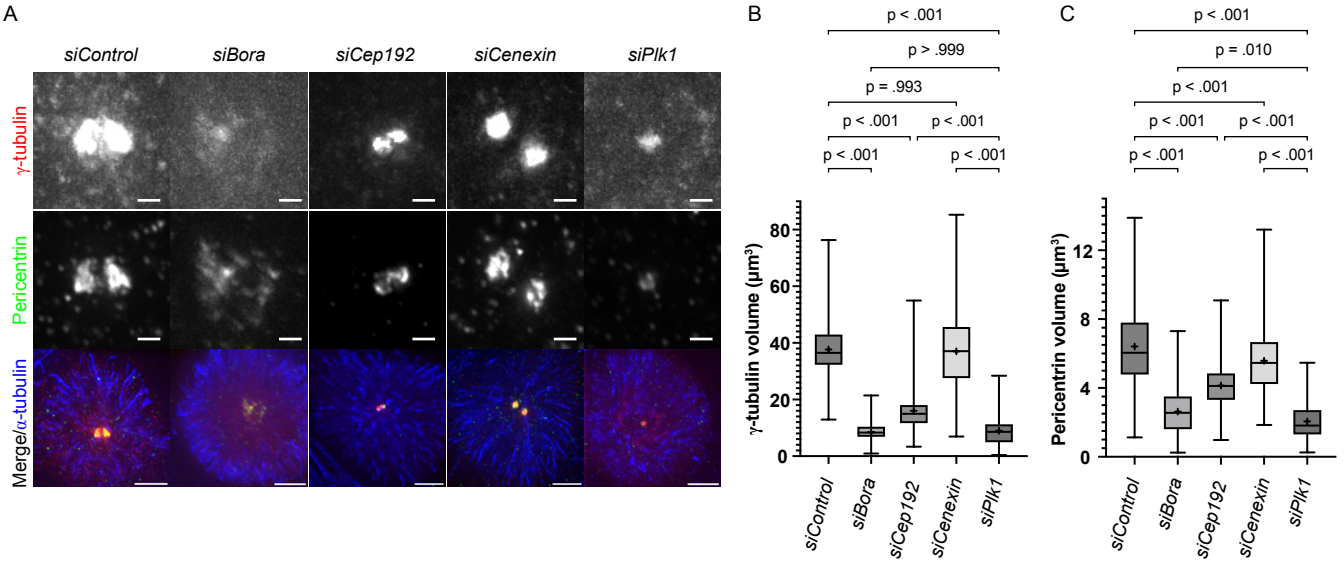

Figure 8. Dwivedi et al.

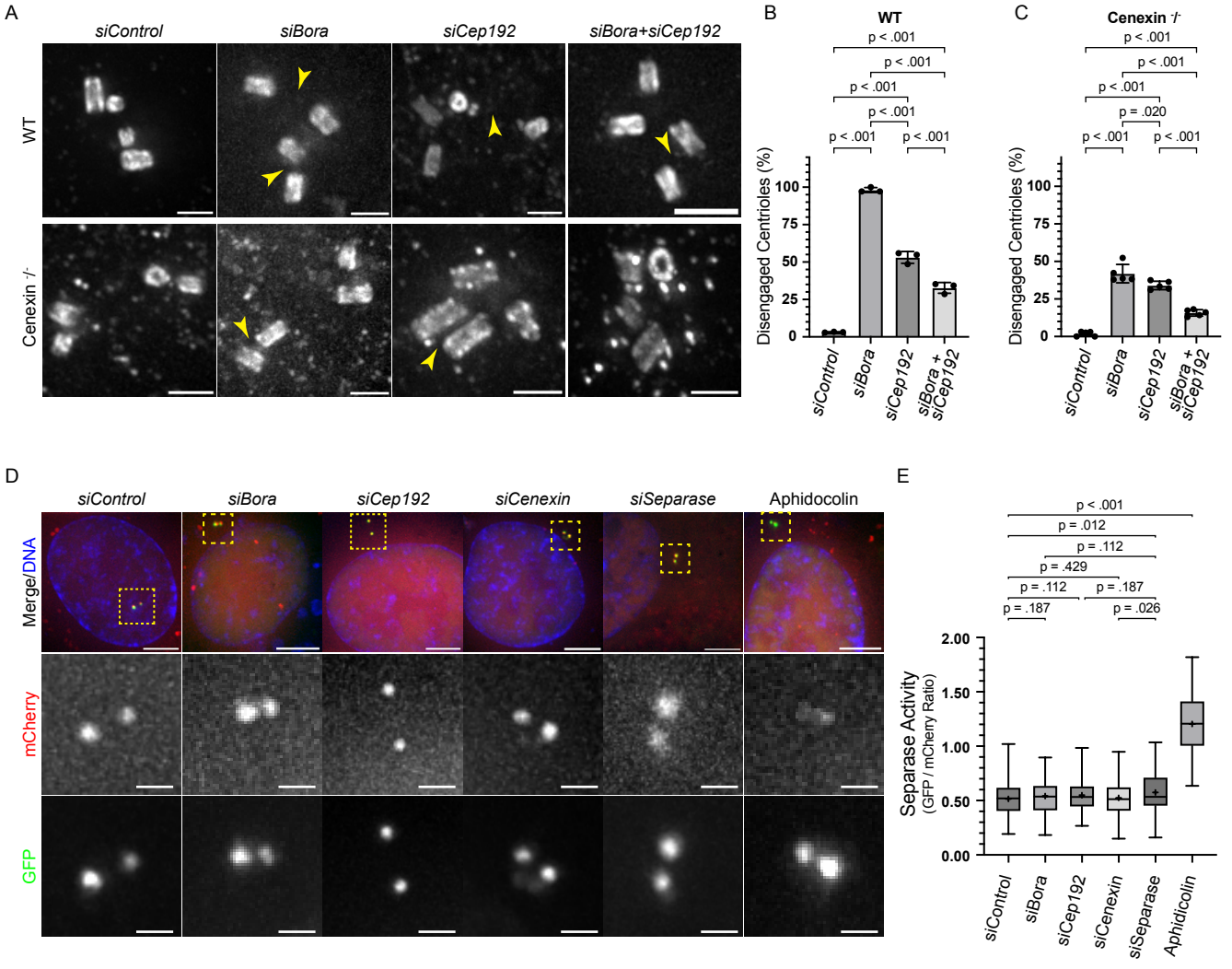

Figure S1. Dwivedi et al.

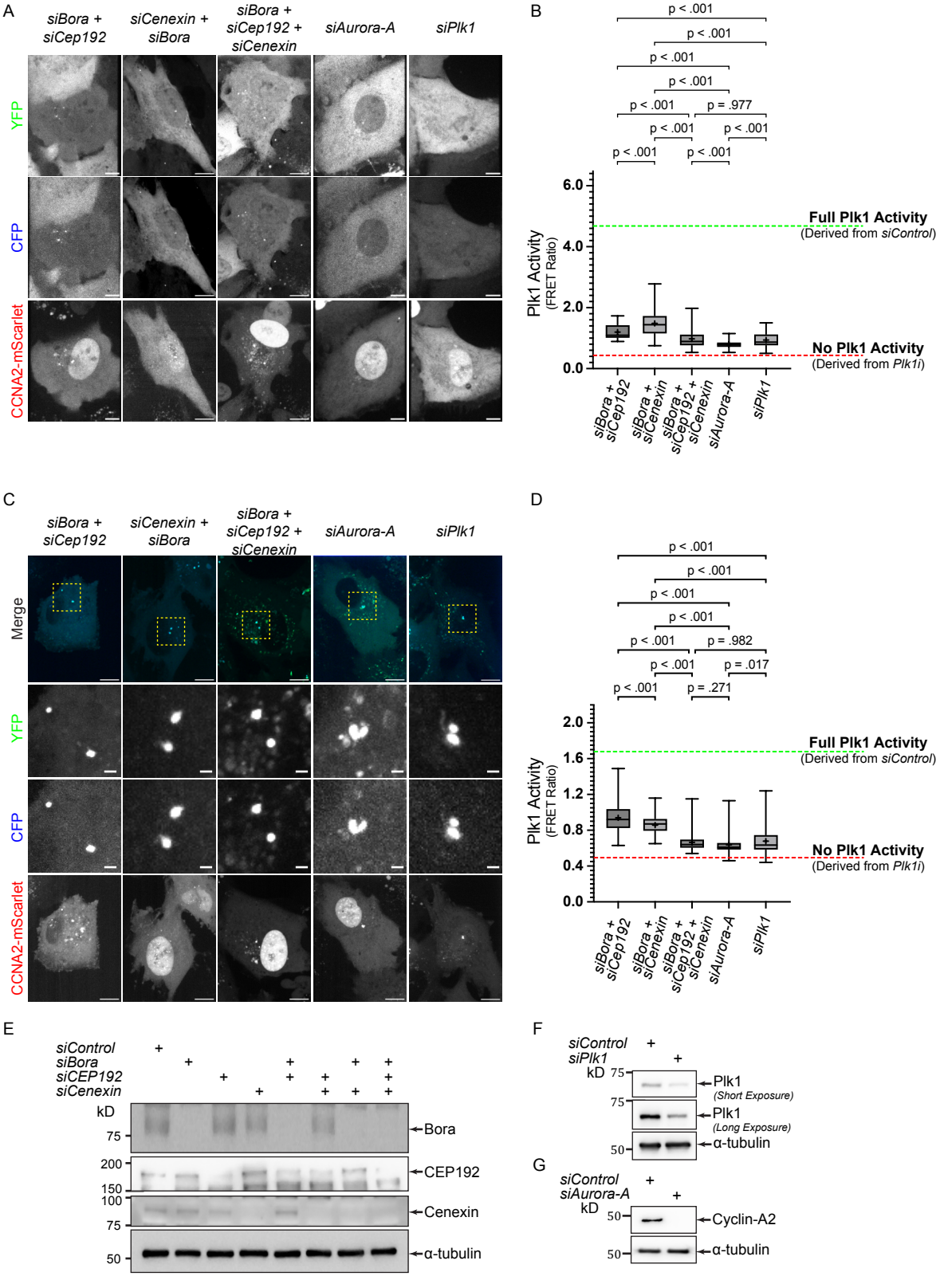

Figure S2. Dwivedi et al.

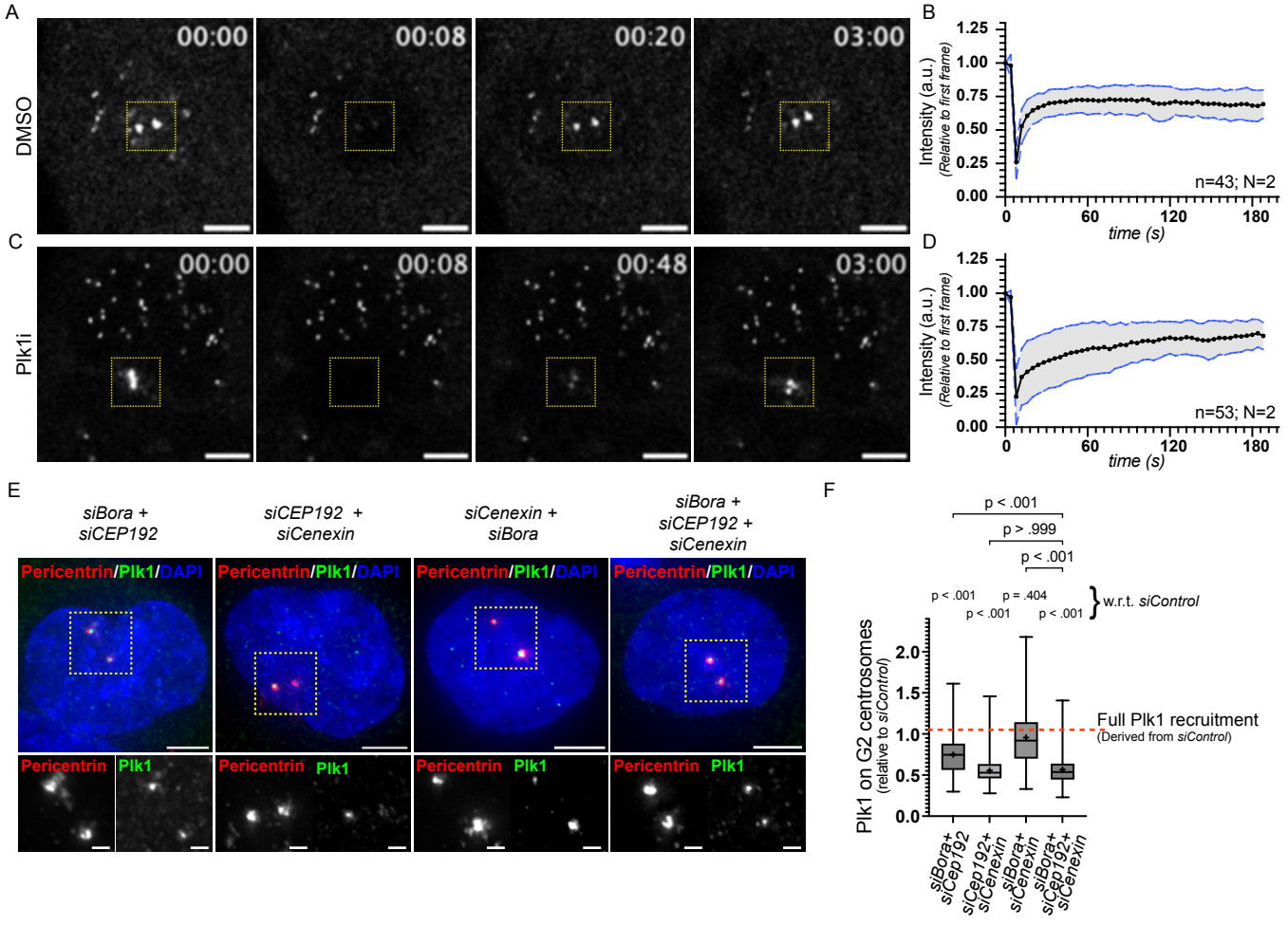

Figure S3. Dwivedi et al.

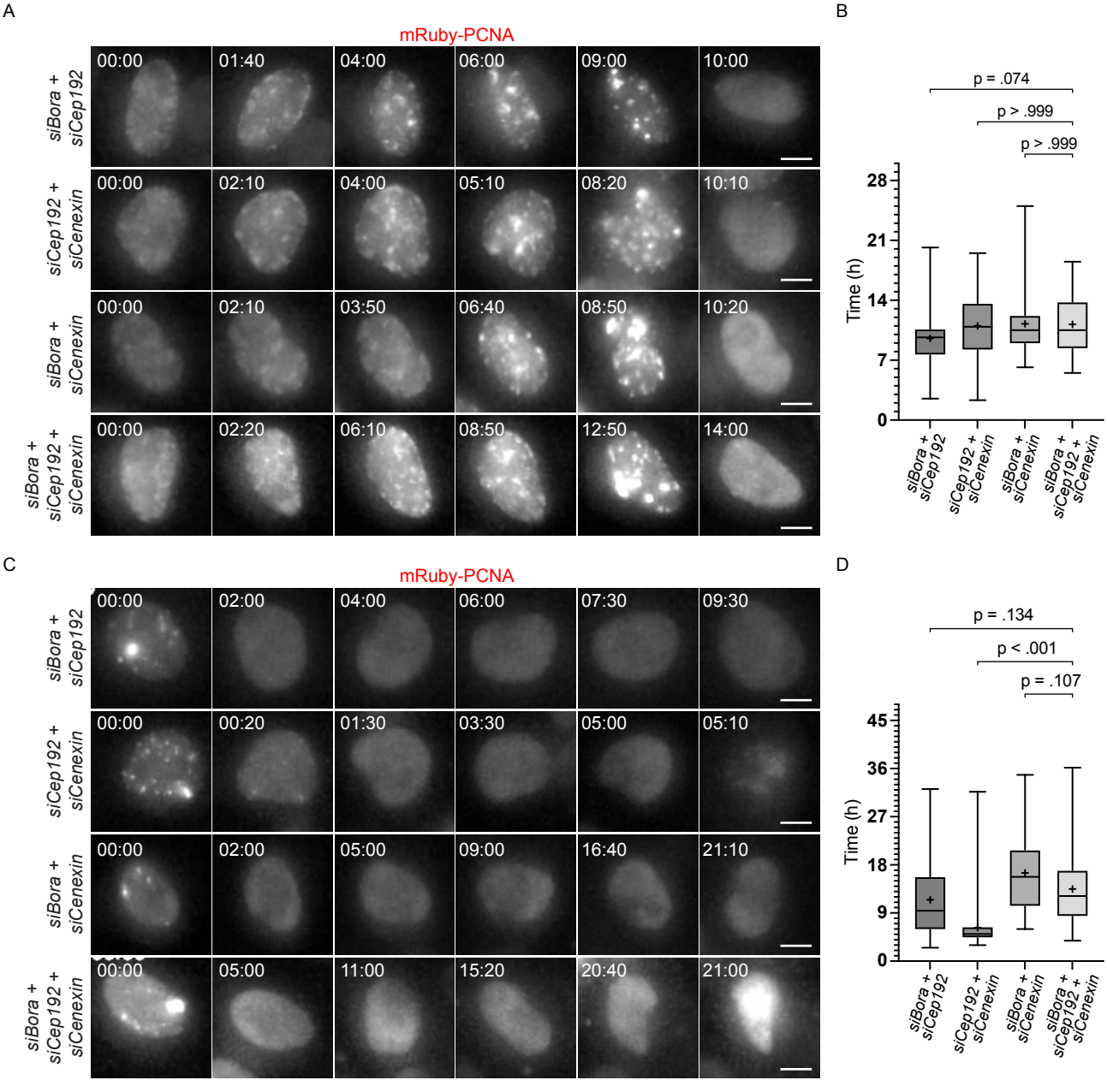

Figure S4. Dwivedi et al.

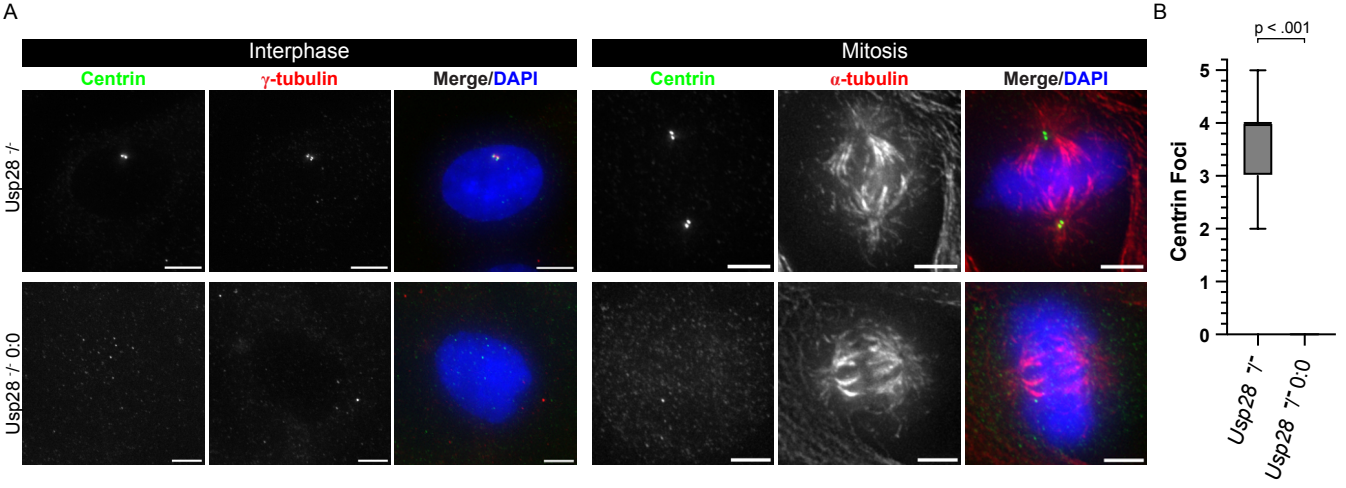

Figure S5. Dwivedi et al.

A

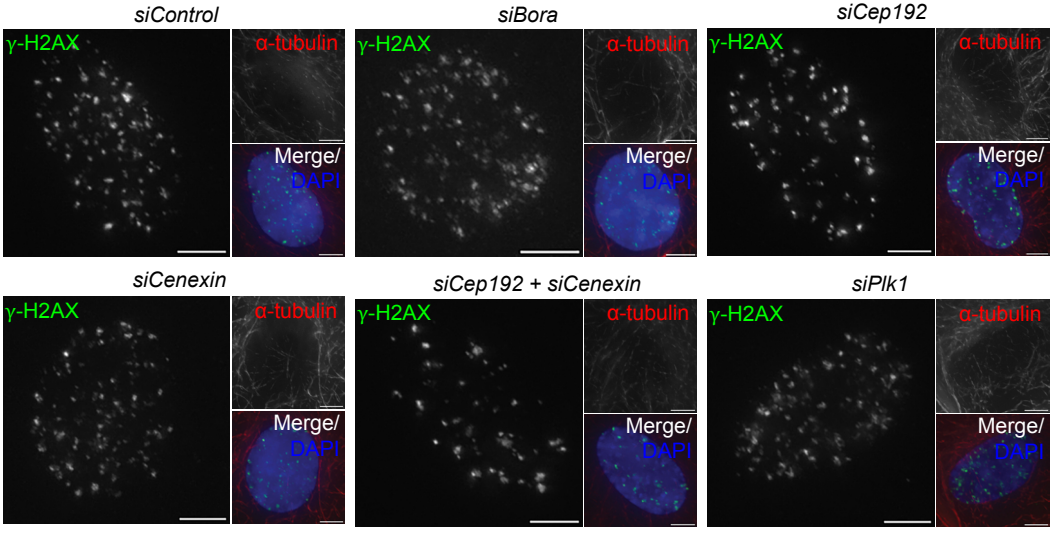

B

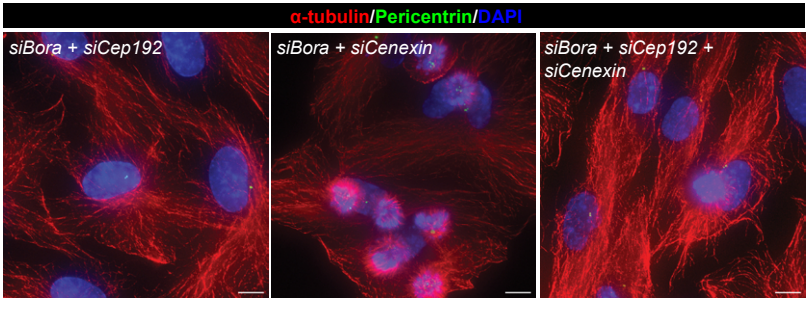

C

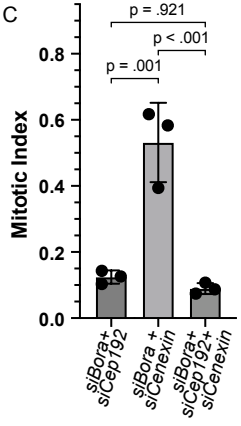

Figure S6. Dwivedi et al.

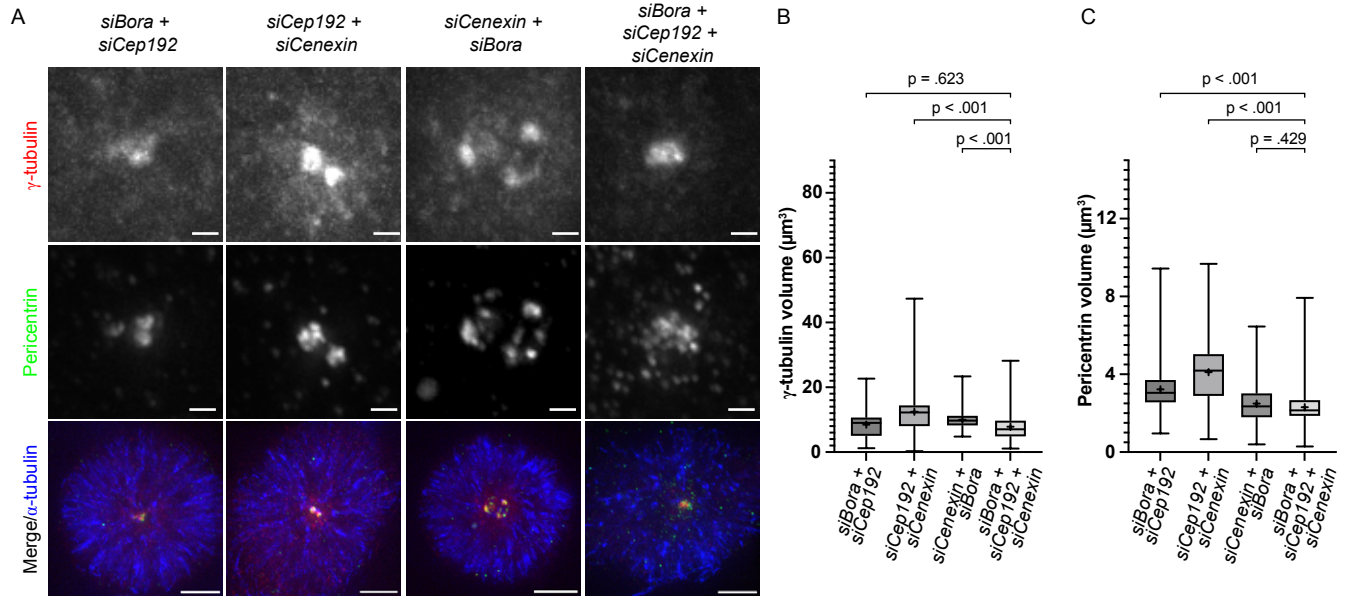
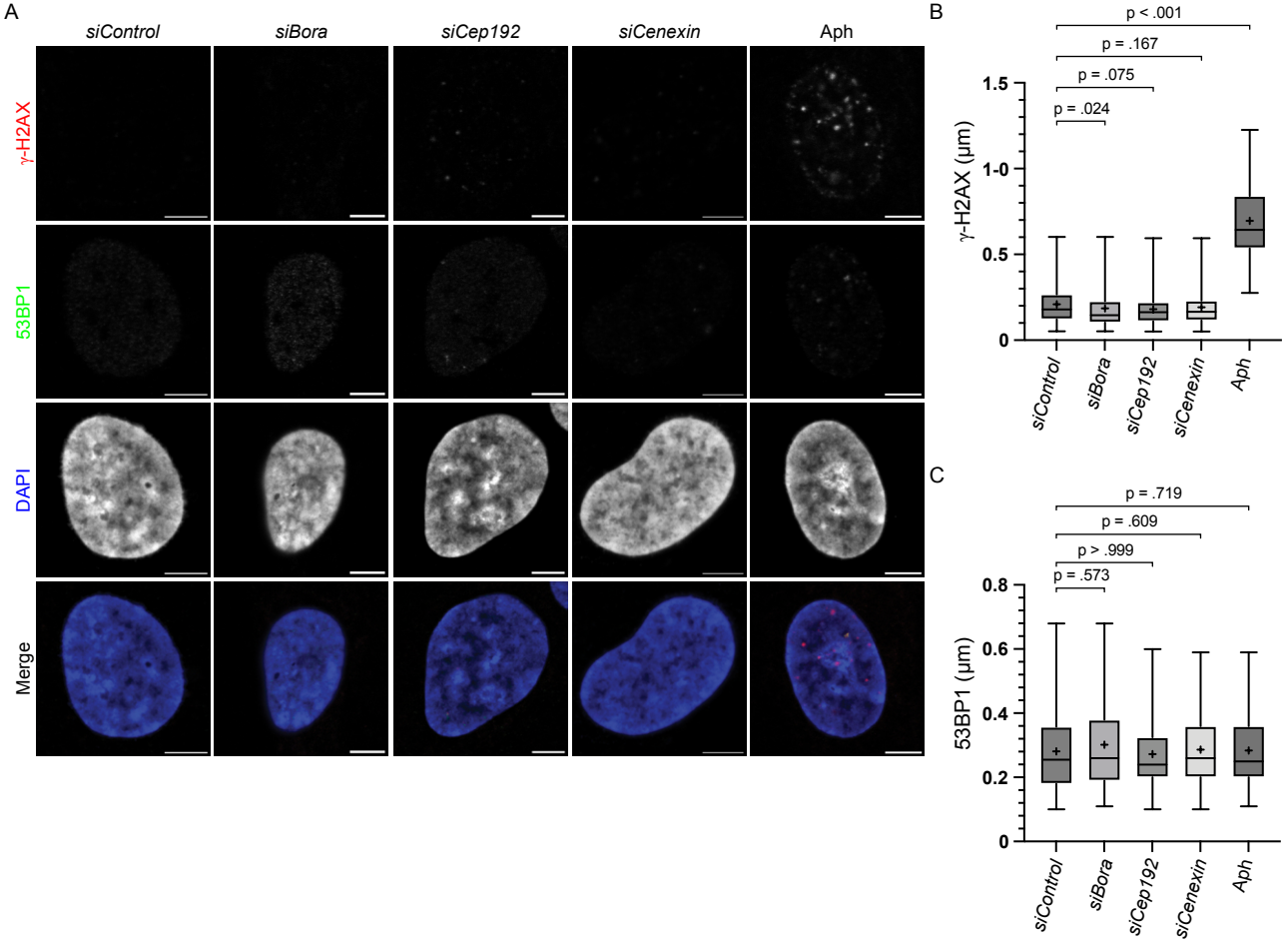
Figure S7. Dwivedi et al.